A lacustrine-based Neoglacial record for Glacier National Park, Montana, USA

Jeffrey S. Munroe [a,*], Thomas A. Crocker [a], Alena M. Giesche [a], Lukas E. Rahlson [a], Logan T. Duran [a], Matthew F. Bigl [a], Benjamin J.C. Laabs [b]

[a] Geology Department, Middlebury College, 276 Bicentennial Way, Middlebury, VT 05753, USA
[b] Department of Geological Sciences, SUNY Geneseo, Geneseo, NY 14454, USA

A B S T R A C T

Multi-proxy study of sediment cores retrieved from lakes below modern glaciers supports the first detailed Neoglacial chronology for Glacier National Park (GNP), Montana. Analysis focused on sedimentary properties sensitive to the extent and activity of upstream glacier ice, including: water, organic matter, carbonate, and biogenic silica content; bulk density; mass accumulation rate; phosphorus fractionation; magnetic susceptibility; L*a*b* color values; and grain size distribution. Results indicate that alpine glaciers in GNP advanced and retreated numerous times during the Holocene after the onset of Neoglaciation ca 6500 BP. The two oldest phases of glacier expansion were synchronous with the well-documented Garibaldi (5600–6900 BP) and Tiedemann-Peyto (1900–3700 BP) phases in western Canada. Younger phases correspond with the First Millennium Advance in western Canada, as well as glacier with advances in the Sierra Nevada. The culminating Little Ice Age (LIA) advance was the most recent and extensive of a series of advance/retreat cycles over the past millennium. Retreat from the LIA maximum was the most dramatic episode of ice retreat in at least the last 1000 years.

© 2012 Elsevier Ltd. All rights reserved.

1. Introduction

Determining the timing, spatial extents, and drivers of climate changes during the Holocene Epoch is a major effort of modern paleoclimate research (e.g. Mayewski et al., 2004; Wanner et al., 2008, 2011). Small alpine glaciers are valuable sources of information because their fluctuations integrate changing climatic conditions with sub-decadal time lags (Jóhannesson et al., 1989; Oerlemans, 2005). Improved understanding of glacier fluctuations during the Holocene Neoglaciation leading up to the culmination of the Little Ice Age (LIA) in the mid-1800s (Grove, 2004), therefore, offers the potential to reveal important information about Holocene paleoclimate variability (Davis et al., 2009).

Records of Holocene glacier fluctuations can be obtained from a variety of sources including glacial landforms, tree-rings, and lake sediments. Glacial moraines offer direct testimony regarding past glacier extents (Schaefer et al., 2009), however, because of obliterative overlap, moraines are often preserved from only the most extensive advance (Gibbons et al., 1984). In most alpine regions worldwide, the most extensive advance of the Holocene occurred during the Little Ice Age, culminating ca AD 1850 (Grove, 2004).

Landforms recording older Holocene advances are correspondingly rare. Tree-ring records developed from wood incorporated into till, and sheared stumps at the base of till units, can provide annually resolved information about the timing of glacier advances (e.g. Luckman, 1995; Holzhauser et al., 2005). However, glacier maxima and intervals of retreat are not represented, and only intervals of glacier extent greater than modern are recorded. Dendrochronology applied to the forefields of glaciers in retreated positions can limit the timing of ice retreat (e.g. Carrara and McGimsey, 1981). However, this approach can be compromised by a variable time-lag between ice retreat and seedling establishment, and is generally only viable for retreat from the LIA terminal position.

Some of the best information about Holocene fluctuations of alpine glaciers is derived from lake sediments (e.g. Leonard and Reasoner, 1999; Nesje et al., 2001). Glacier activity exerts a first-order control over the properties of sediment accumulating in downstream lakes (Karlén, 1981). Thus, if a glacier meltwater stream enters a perennial lake with no potential for bypassing, then fluctuations of that glacier will be recorded in the lacustrine sedimentary record. Lacustrine sediments also offer the potential for identifying advances of upstream glaciers to positions not represented in the geomorphic record.

This study developed records of Holocene fluctuations of several glaciers in Glacier National Park (GNP), Montana, USA, to provide a context in which to evaluate the observed record of glacier

retreat. Overall, GNP offers a particularly vivid example of recent changes in the cryosphere, with a reduction in glacier area of >36% since AD 1850 (Key et al., 2002). Looking forward, numerical modeling experiments predict that glaciers may disappear entirely from GNP by AD 2030 (Hall and Fagre, 2003), although other models suggest ice may persist through the middle of this century (Brown et al., 2010).

Such dramatic glacier retreat is frequently highlighted as a signal of global warming (e.g. Appenzeller, 2007), but in reality very little is known about fluctuations of glaciers in GNP before the LIA. It has long been assumed that modern glaciers in GNP formed after the early Holocene Altithermal (Matthes, 1940), but this theory has never been tested. Subdued moraines near the margins of some modern glaciers likely formed during the Younger Dryas (YD) chronozone in the latest Pleistocene (MacLeod et al., 2006), and a second set of less-weathered moraines was deposited up-valley of these during the local LIA maximum (Carrara, 1987). Recent study of a sediment core from Swiftcurrent Lake on the east side of GNP provides some constraints on Holocene activity of the Grinnell Glacier (MacGregor et al., 2011), however there has been no focused effort to construct a chronology for glacier fluctuations in GNP for the millennia between the YD and the LIA. As a result, a temporal context in which to consider contemporary retreat of these glaciers is lacking. Furthermore, despite the ongoing glacier recession, GNP remains a localized outpost of glacierization in a region of mostly ice-free mountain ranges (Key et al., 2002), and a Neoglacial record for GNP would be a valuable point of comparison with records previously developed for elsewhere in western North America (e.g. Barclay et al., 2009; Menounos et al., 2009; Bowerman and Clark, 2011; Osborn et al., 2012). Integrated consideration of multiple records from the region may also illuminate regional patterns and periodicities reflecting the operation of different climatic drivers (Wanner et al., 2008, 2011).

2. Setting and field methods

2.1. Setting

The field strategy for this project involved the collection of sediment cores from lakes located downstream from modern glaciers. Lakes were selected with the goal of distributing study sites on either side of the Continental Divide, and along the north–south extent of the glacierized region within GNP. Proximity of each lake to upstream glaciers was considered, as it was expected that lakes closer to glaciers would record a stronger signal of glacier fluctuations. Because the fieldwork took place in designated wilderness areas within a national park, motorized equipment was prohibited and lakes had to be accessible for pack animals to carry the coring equipment. Prohibitions on pack animal access to some areas, and limits on the distance that the animals could safely travel in a day (in locations where overnight backcountry stays were prohibited) also precluded access to some lakes.

After consideration of all these constraints, four lakes were selected (Table 1):

1) In the northwest corner of GNP cores were retrieved from the east end of Upper Kintla Lake (UKL) below the Agassiz Glacier (Fig. 1). The Agassiz Glacier was one of the largest in GNP at the peak of the LIA. Field reports, photographs, and a well-preserved terminal moraine loop indicate that the glacier flowed out of its cirque and extended downslope into the forest. In contrast, by AD 1993 the glacier covered just 1.02 km^2, which is 25% of its LIA extent (Key et al., 2002), and had lost more than 90% of its former volume (Carrara and McGimsey, 1981). The glacier occupies the southwestern corner of

Table 1
Dimensions of studied lakes, glaciers, and cores collected from Glacier National Park.

Lake		UKL-1	UKL-3	Cracker	Cosley	Harrison
Glacier		Agassiz		Siyeh	Whitecrow[a]	Harrison
Location in GNP		NW		SE	NE	SW
Elevation	m	1345		1819	1490	1137
Max Depth	m	56		17	36	42
Lake Area	ha	190		1.6	9	160
Watershed	km^2	84.4		19	75.6	70.4
Ice Area (yr)	acres	991 (1993)		53 (1966)	457 (1966)	1462 (1993)
Ice Cover[b]	%	4.8		1.1	2.4	8.4
Glacier Distance	km	5.2		0.9	5.2[c]	8.7
Core Latitude (N)	DD.ddd	48.976	48.980	48.745	48.925	48.524
Core Longitude (W)	DD.ddd	114.150	114.156	113.643	113.747	113.760
Water Depth	m	4.9	35.7	15.8	13.4	32.5
Core Length	m	3.83	3.24	3.19	5.34	6.18
Max sed rate	mm/yr	24.4	1.1	2.9	0.7	8.4
Min sed rate	mm/yr	2.3	0.4	0.8	0.1	1.1
mean sed rate	mm/yr	3.4	0.5	1.3	0.3	1.6

[a] And other glaciers at the head of the Mokowanis River drainage.
[b] Total upstream ice cover as percent of watershed area.
[c] Mokowanis inflow first passes through Glenns Lake.

a cirque developed to the east of Kintla Peak (3079 m asl) and is underlain by carbonate bedrock of the Helena Formation (Whipple, 1992). Meltwater from the glacier drops ~900 m in 5 km through Agassiz Creek to Upper Kintla Lake, which covers 1.9 km^2 with a maximum depth of 56 m (Table 1).

2) Harrison Lake was selected to represent the southwest corner of GNP (Fig. 1). The eastern end of this lake receives meltwater and sediment directly from the Harrison Glacier. This glacier, with an area of 1.06 km^2 in AD 1993, is one of the largest remaining in GNP (Key et al., 2002). It is also one of the highest glaciers in GNP with a mean elevation of ~2550 m. It rests primarily on argillite of the Empire and Grinnell Formations (Whipple, 1992) and faces southeast. Harrison Lake, with an area of 1.6 km^2 and a maximum depth of 42 m, is located ~10 km downstream from the glacier (Table 1).

3) Cracker Lake was cored in the southeastern corner of GNP (Fig. 1). This lake was the smallest in the study (0.16 km^2, maximum depth of 17 m). Cracker Lake is also located the shortest distance away from an upstream glacier; the Siyeh Glacier extends to within 1000 m of the southwestern end of the lake, and the LIA terminal moraine of this glacier is only 450 m from the lakeshore (Table 1). The small Siyeh Glacier (0.22 km^2 in AD 1966) sits on carbonate bedrock of the Helena Formation and argillite of the Empire Formation (Whipple, 1992) at an average elevation of 2070 m, with an aspect of north-northeast (Table 1).

4) Cosley Lake was selected to represent the northeastern corner of GNP (Fig. 1). This lake receives meltwater from numerous glaciers in the headwaters of the Mokowanis River ~10 km upstream. The lake, which covers an area of 0.9 km^2 to a maximum depth of 36 m, is fed by the Mokowanis River, which passes through Glenns Lake before entering Cosley (Table 1). Upstream glaciers rest on argillite of the Snowslip Formation and carbonate of the Helena Formation (Whipple, 1992). Remnants of the former Whitecrow Glacier to the northwest of the lake rest on carbonate of the Helena formation (Whipple, 1992) and drain directly to Cosley via Whitecrow Creek, which constructed the large alluvial fan that separates the two lakes (Fig. 1).

2.2. Field methods

Prior to coring, bathymetric maps were constructed for each lake using a Humminbird sonar and GPS receiver to collect several hundred georeferenced depth measurements. These points were
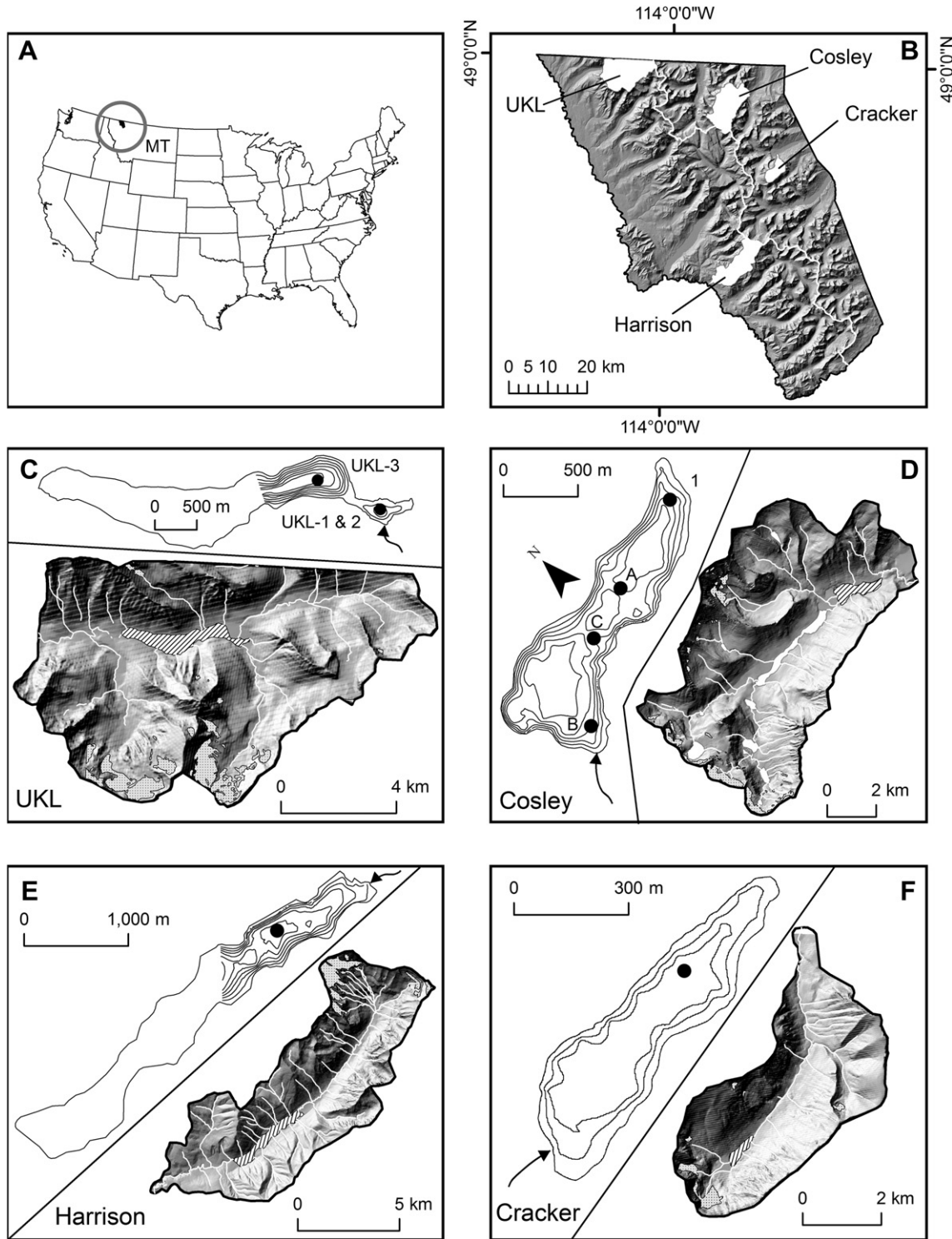
Fig. 1. Location map of the study area and cored lakes. Panel A. Location (circled) of Glacier National Park (GNP) in northwestern Montana (MT), USA. Panel B. Outlines of the four studied watersheds (labeled) superimposed on a shaded topographic model of GNP. The solid white line denotes the continental divide. Panels C through F. Detailed views of the watershed surrounding each lake. Arrows denote inflowing streams. Glaciers are denoted with a stippled pattern, while cored lakes are designated by black diagonal lines. Enlargements of each lake present mapped bathymetry (only the eastern sectors of Upper Kintla and Harrison Lakes were mapped) along with coring locations (circles). North is toward the top of the page for all maps except the enlargement of Cosley Lake (noted). The interval for the bathymetric contours is 6 m (20 ft).

gridded using a kriging function and displayed in ArcMap 9.3 running on an xPlore tablet PC with integrated GPS. This approach allowed the position of the coring platform to be displayed in real-time over the interpolated bathymetric map, facilitating selection of a coring site with appropriate water depth and bottom topography.

Three different coring techniques were employed from a floating platform to yield continuous sedimentary records extending from the sediment–water interface to the point of refusal, or the limit of the coring equipment. A UWITEC Complete Corer was used to collect undisturbed near-surface sediment, penetrating 20–75 cm into the sediment of Harrison and Cosley

Lakes, and at one location in Upper Kintla Lake. However, the sediment elsewhere in Upper Kintla Lake, as well as in Cracker Lake, proved too stiff for this lightweight gravity corer, so a Livingstone corer fitted with a clear plastic tube was used to retrieve the sediment–water interface. Surface cores obtained with these methods were subsampled at 1-cm intervals into whirlpak sample bags.

A 5-cm diameter Livingstone corer (Livingstone, 1955) with a metal barrel was used to retrieve core segments overlapping with the sediment retrieved by the UWITEC, and extending down to ∼100 cm below the surface. Livingstone cores were extruded, wrapped in saran and aluminum foil, cut to 50-cm lengths, and stored in collapsible core boxes.

Finally, a modified Reasoner-type percussion corer (Reasoner, 1993) outfitted with a cable-actuated piston, tapered steel nose-cone, and integrated core catcher was used to collect sediment down to the point of refusal. The percussion corer utilized a 6-m long core barrel of 7.5-cm diameter PVC pipe. Driving of the percussion corer began at the sediment–water interface, but the unconsolidated near-surface sediment was impossible to retrieve without disturbance with this method. The driving weight was a 1.5-m long section of 10-cm diameter high-impact PVC filled with sand and gravel from the lakeshore. Filled sections of percussion core were cut to ∼80-cm lengths, fitted with plastic caps, and sealed for transport from the backcountry on pack animals. All cores and samples were ground-shipped back to Middlebury College and stored at 4 °C until analysis.

2.3. Lab methods

All cores were analyzed for multiple properties sensitive to the extent and behavior of glacier ice upstream. Before opening, core sections were X-rayed and run through a Bartington Magnetic Susceptibility (MS) meter connected to a 12-cm diameter loop for measurement at 1-cm intervals. The MS meter was re-zeroed every 50 cm and a drift correction was applied to all measurements.

Percussion core sections were opened by cutting the PVC lengthwise with a circular saw and pulling a thin wire from top to bottom. Livingstone core sections were unwrapped and split with a knife. Freshly opened cores were photographed and visual stratigraphy was recorded. One section was tightly wrapped in a single layer of saran and properties of light reflected off the sediment were determined with a Konica-Minolta CM-2600D color spectrophotometer (CSP). Three measurements were taken every cm and averaged to provide values with 1-cm resolution. Color values are reported using the CIELAB L*a*b* system where L* is luminosity from 0 (black) to 100 (white), a* is a measure of redness (positive values) to greenness (negative values), and b* is a measure of yellowness (positive values) to blueness (negative values). After the CSP analysis, this half of each core section was wrapped in 46-gauge Saran 8, and heat-sealed inside a shrink-wrap sleeve before being archived at 4 °C.

The other half of each section was sampled at 1-cm resolution in quadruplicate. Water content, loss-on-ignition (LOI) at 550 °C (LOI-550), and LOI at 1000 °C (LOI-1000) were determined with a Leco TGA 701 thermogravimetric analyzer. LOI-550 is considered a proxy for organic matter content, while LOI-1000 reflects the abundance of carbonate (Dean, 1974). Water content, which reflects bulk density (Menounos, 1997), was determined from the mass lost during heating to 105 °C under a full nitrogen atmosphere for 4 h. LOI-550 was determined from mass lost from the dried sample during 3 h of heating under ambient atmosphere. The 1000 °C step was maintained for 1 h. Actual percent carbonate values were calculated from LOI-1000 estimates with a transfer function generated through analysis of 32 samples with quantitative X-ray

diffraction. This analysis revealed a strong linear correlation ($r^2 = 0.8$) between the two estimates of carbonate abundance, with true carbonate content corresponding to 2.3-times LOI-1000.

Biogenic silica (bSi) content was determined for freeze-dried samples by sequential extraction while leaching in 0.1 M NaOH for 5 h at 85 °C (DeMaster, 1981). Dissolved Si content was determined for each aliquot by spectrophotometry at 812 nm after addition of reagents for a molybdate blue reaction (Strickland and Parsons, 1965). The %bSi was calculated from the y-intercept of a linear function fit to the results for extractions for hours 2 through 5. Analysis of replicates indicates that this method has a reproducibility of 10%. Bulk density (BD) was determined from the wet volume and freeze-dried mass. A known-volume sampler (3-cm^3) was used for the cores from Upper Kintla Lake, while a Quantachrome Pentapycnometer was used to determine volumes for samples from the other lakes. Grain size (GS) distribution was determined with laser scattering in a Horiba LA950 after treatment with 35% H_2O_2 (3 additions of 10 ml over 7–10 days) to remove organic matter and 0.1 M NaOH (1 h, 85 °C) to remove biogenic silica. Sodium hexametaphosphate (3%) was used as a dispersant. The relative abundances of Fe-occluded (Fe–P), mineral (mP), and organic-bound (org-P) phosphorus were determined at 2-cm intervals for core UKL-3 and 4-cm intervals for core UKL-1 through sequential extraction and analysis via ICP-AES and spectrophotometry (Filippelli et al., 2006).

A variety of geochronology approaches was utilized to convert the multi-proxy results to time series. A total of 31 terrestrial macrofossils, including *Picea englemannii* needles and cones, twigs, and bulk sediment was submitted for AMS radiocarbon dating. Radiocarbon results were converted to calendar ages with Calib 6.0 (Stuiver and Reimer, 1993), using the Intcal09 calibration curve (Reimer et al., 2009). The age with the median probability was used for developing age-depth models. A prominent ash layer from a depth of 164–177 cm in the core from Cosley Lake was submitted to the USGS Tephrochronology Lab for geochemical fingerprinting. Subsamples from the top ∼80 cm of the UKL-1 core were analyzed for dating with ^{210}Pb. The upper 38 cm of the core from Cracker Lake were analyzed with ICP-AES to search for a spike in Cu, to correlate with AD 1901, when records indicate a copper mine operated briefly along the southern shore of the lake (Higgins, 1998).

Measured BD values were combined with sample resolutions from the depth-age models to calculate sedimentary fluxes of bSi and $CaCO_3$ for each record in mg/cm^2/yr. A mass accumulation rate (MAR) of clastic sediment [i.e. 100 − (%OM + %bSi)] was also calculated in gm/cm^2/yr.

3. Results

3.1. Coring

Coring locations and information about the lengths of the resulting cores are provided in Table 1. Three cores were retrieved from Upper Kintla Lake: two from the sub-basin directly in front of the inlet from the Agassiz Glacier (UKL-1 and UKL-2), and a third (UKL-3) from deep water (35.7 m) at the eastern end of the main lake (Fig. 1C). A Livingstone corer with a clear tube was used to collect an intact sediment–water interface for cores UKL-1 and UKL-2, and the UWITEC Complete Corer was used to retrieve a sample of the surface sediment for core UKL-3.

Cosley Lake was cored at its extreme east end (#1 in Fig. 1D) to avoid the influence of the inflowing Mokowanis River while remaining in a workable water depth (13.4 m). The core was collected from an extensive shelf perched slightly above the floor of the eastern basin of the lake. Again the Livingstone corer with

a clear tube was used to collect the sediment−water interface. The UWITEC corer was also used to collect surface sediment at 3 other locations along the axis of the lake to assess homogeneity of the near-surface sediment (A, B, and C in Fig. 1D).

Harrison Lake was cored in an area of relatively flat bathymetry at the eastern end of the lake, 850 m southwest of the inlet stream (Fig. 1E). The water depth at this location (32.5 m) was too great for the Livingstone corer, however the UWITEC was capable of penetrating the near-surface sediment.

Cracker Lake was cored near its eastern end in a location selected to minimize the influence of sediment delivery from prominent debris-flow gullies (Fig. 1F). The UWITEC corer was unable to penetrate the stiff near-surface sediment in this lake. However, the water depth (15.8 m) at the coring site was shallow enough to allow use of the Livingstone corer with a clear tube to retrieve the sediment−water interface.

3.2. Stratigraphy

Cores reached depths from 319 cm (Cracker Lake) to 618 cm (Harrison Lake) below the sediment−water interface (Table 1). Coring stopped at the point of refusal in all lakes except Harrison, where coring was limited by the length of the available core barrel.

Cores UKL-1 and UKL-2 exhibited a nearly identical stratigraphy featuring generally reddish black (2.5Y 2.5/1) to reddish gray (2.5Y 5/1) silty clay interrupted by thin (<1 cm) darker layers rich in organic matter. Given the strong similarity between these cores and their resulting proxy time-series, only UKL-1 is presented and interpreted in this paper.

Core UKL-3 featured laminated dark gray (5Y 4/1) silty clay, locally interrupted by bands (∼2−4 cm thick) of very dark gray (2.5Y 3/1) sediment. Also notable was the presence of strongly contrasting layers of green sediment 0.2−0.5 cm thick, which under magnification were found to be composed almost entirely of finely ground fragments of green argillite, likely derived from the Appekunny Formation that outcrops in the valley walls above the lake (Whipple, 1992). The bottom ∼20 cm of this core were lighter colored, slightly coarser, and featured a characteristic gritty texture. Under magnification this light-colored sediment was shown to be rich in glass shards.

The core from Cracker Lake exhibited alternating gray (10YR 5/1) and weak red (2.5YR 4/2) layers throughout. Gas bubbles were present in the uppermost 30 cm of the core, while the bottom ∼5 cm was dense, dry, and sandy. Stone chips and pebbles to ∼2-cm in diameter were common throughout the core.

The Harrison Lake core was uniform, massive, and vesicular throughout. Munsell color was consistently dark gray (7.5YR 4/1), except for the deepest ∼150 cm, which featured gray (5YR 5/1) alternating with weak red (2.5YR 5/2) layers roughly 5 cm thick.

The core from Cosley Lake featured the most dramatic stratigraphic variability. Above a depth of 164 cm, dark gray (10 YR 4/1) silty clay alternated with gray (5 YR 5/1) layers. A slightly contrasting gray (10 YR 5/1) sandy layer from 164 to 177 cm contained abundant glass shards 10−100 μm in length. The base of this layer was extremely coarse, with a median grain size of 40 μm and a sand fraction of ∼60%. Beneath this layer weak red (2.5YR 5/2) silty clay alternated with darker (10YR 4/1) sediment for ∼100 cm. The base of this section transitioned gradually to reddish gray (2.5YR 5/1), sticky, very fine silty clay that continued to almost the bottom of the core. The lowest 13 cm was a dense, gravelly, reddish gray (5YR 5/2) diamicton.

3.3. Geochronology

Results of the radiocarbon dating of 31 samples from these cores are presented in Table 2. The majority of samples were terrestrial macrofossils, which are unaffected by potential hard water effects. However, a lack of terrestrial material in the lower part of the Cosley Lake core necessitated dating of dispersed organics for the deepest sample (Cosley 280-284). As a check for potential bias of the resulting age, a pair of ages was determined on concentrated aquatic organics (Cosley_67-bulk) and a small piece of wood from a depth of 67 cm (Cosley_67). The resulting difference in age of these samples (1090 ^{14}C years) suggests that old carbon is artificially skewing the age of aquatic organic matter. Thus, the deepest age from this lake was adjusted by 1090 ^{14}C years in the age model.

Two samples contained radiocarbon concentrations above modern levels, indicating that the dated organisms were living during the peak of atmospheric bomb testing in the mid-20th Century. Conifer needles and a wood fragment from a depth of 12 cm in the core from Harrison Lake (Harrison-12) returned a value of 119.9 pMc. This result corresponds to an age of AD 1958 to AD 1987 according to the Bomb 04 NH1 calibration curve in OxCal (Ramsey, 2006). A second sample from near the top of core UKL-2 (UKL-2_21) returned a result of 138.6 pMc, which corresponds to an age of AD 1962−AD 1976.

The lone chronologic inversion in the study was encountered in core UKL-3. When this core was opened, a prominent discontinuity was revealed cutting across the visible stratigraphic layers at a depth of 62 cm. The origin of this feature was unclear, however it was suspected that it may have been produced by a subaqueous slump that disturbed the upper part of the stratigraphic section. The radiocarbon results (Table 2) confirm the presence of repeated stratigraphy above this discontinuity, so all sediment above the 62-cm depth was ignored and this depth was established as the new zero reference for all other samples (sample UKL-3_0). This conservative approach results in artificial truncation of the sediment record but avoids potential issues associated with disturbed stratigraphy near the core top. The remaining radiocarbon analyses for core UKL-3 are in stratigraphic order (Table 2) with the zero depth corresponding to ∼1000 years BP and the core bottom to 7700 years BP. Glass shards are present in the basal sediments, which are assumed to represent the Mazama tephra given the result (7630 BP) for the near-basal sample UKL-3_315.

Analysis of the upper 38 cm of the Cracker Lake core with ICP-AES revealed a spike in Cu abundance more than 2 standard deviations above the mean value 11 cm below the sediment−water interface. This spike is assumed to represent the onset of copper mining on the lakeshore (Higgins, 1998). Accordingly, in establishing the depth-age model for this core, an age of AD 1901 was assigned to this depth, which matches well with the age estimate from the ^{14}C results.

The major element composition of the tephra layer encountered in the core from Cosley Lake, determined through electron microprobe analysis, exhibited a very strong match ($r^2 = 0.99$) with the Mazama tephra. In building the depth-age model for this core, the thickness of this ash layer was removed from the stratigraphy, and an age of 7630 BP was assigned to this depth to represent the calendar age of the Mazama eruption (Zdanowicz et al., 1999).

Samples from the upper 80 cm of the UKL-1 core were analyzed for ^{210}Pb abundance. The results demonstrate an exponential decrease in ^{210}Pb concentration with depth, with a depth of 20 cm corresponding to AD 2000, 66 cm corresponding to AD 1950, and 80 cm corresponding to AD 1872. Errors on these results are less than 1 year back to ∼AD 1990, less than 10 years back to AD 1965, and less than 30 years back to AD 1870.

A dense diamicton encountered at the base of the core from Cosley Lake underlies a thick sequence of fine sediment with very low organic content. This deepest sediment is interpreted as glacial till. The age of terminal Pleistocene deglaciation in the Mokowanis

Table 2
Radiocarbon ages for Lake cores from Glacier National Park.

Sample	Lab Code	Material	$d^{13}C$	^{14}C age yr‰	± yr	Calibrated age ranges (yrs)[a]				
						Min	Max	Prob.	Median prob.	Depth cm
Cosley_10	B-28731	Needles	−27.5	4200	40	4586	4596	0.012		41
						4613	**4766**	**0.702**	**4731**	
						4783	4848	0.286		
Cosley_67	B-28731	Stick	−25.8	5320	40	**5991**	**6211**	**0.979**	**6097**	98
						6247	6265	0.021		
Cosley_67-bulk	B-28731	Organics	−28.6	6410	40	**7271**	**7420**	**1.000**	**7350**	98
Cosley_192	B-28731	Stick	−25.3	9730	50	10,876	10,941	0.079		223
						11,078	**11,243**	**0.921**	**11,173**	
Cosley_280-284	B-28731	Organics	−24.9	10,310[b]	50	11,843	11,860	0.012		313
						11,969	**12,237**	**0.750**	**12,118**	
						12,242	12,388	0.238		
Cracker_11	B-28507	Needle	−27.4	190	40	−3	35	0.179		30
						70	117	0.072		
						132	**229**	**0.513**	**178**	
						251	305	0.236		
Cracker_75	B-28507	Stick	−28.3	630	40	**549**	**665**	**1.000**	**602**	94
Cracker_145	B-28507	Wood	−24.6	1240	40	**1068**	**1270**	**1.000**	**1179**	164
Cracker_220	B-28507	Wood	−23.9	1620	40	**1409**	**1606**	**1.000**	**1504**	239
Cracker_279	B-28507	Stick	−24	2100	40	1950	1961	0.011		298
						1969	1979	0.010		
						1985	**2155**	**0.945**	**2073**	
						2269	2295	0.034		
Harrison_12	B-287317	Needles	−25.6	119.9 pMc	0.4	**−8**	**−37**	**1.000**	**−23**	23
Harrison_103	B-28731	Stick	−30.2	540	40	**509**	**564**	**0.614**	**552**	114
						588	642	0.386		
Harrison_236	B-28731	Wood	−24.2	1690	40	**1524**	**1701**	**1.000**	**1598**	247
Harrison_460	B-28732	Wood	−23.6	3010	40	**3078**	**3335**	**1.000**	**3216**	471
Harrison_586	B-28732	Cone	−23.5	3490	40	3643	3664	0.039		597
						3683	**3867**	**0.961**	**3765**	
UKL-1_39	OS-66109	Stick	−27.18	145	30	−3	0	0.007		53
						2	41	0.171		
						59	**153**	**0.349**	**147**	
						169	233	0.304		
						240	282	0.170		
UKL-1_131	OS-66681	Needle	−28.42	300	45	158	163	0.007		145
						286	**482**	**0.993**	**383**	
UKL-1_230	OS-66573	Needles	−26.69	655	45	**551**	**675**	**1.000**	**610**	244
UKL-1_325	OS-66992	Needle	−28.97	1030	75	**766**	**1091**	**0.981**	**945**	339
						1107	1134	0.017		
						1163	1167	0.002		
UKL-2_21	OS-66110	Needles	−30.3	138.6 pMc	0.56	**−12**	**−26**	**1.000**	**−18**	50[c]
UKL-2_96	OS-66574	Needle	−29.45	35	35	−5	−2	0.061		88[c]
						31	**84**	**0.508**	**68**	
						87	138	0.214		
						223	256	0.217		
UKL-2_161	OS-66111	Needles	−26.84	280	25	159	162	0.003		150[c]
						286	332	0.447		
						355	**433**	**0.550**	**373**	
UKL-2_274	OS-66682	Needles	−26.79	575	45	523	574	0.378		215[c]
						576	**653**	**0.622**	**598**	
UKL-2_412	OS-66088	Needles	−25.04	915	25	**768**	**918**	**1.000**	**851**	309[c]
UKL-3_char	OS-66652	Charcoal	−23.36	1840	35	**1704**	**1869**	**1.000**	**1777**	−
UKL-3_0	OS-66712	Needles	−26.98	1060	0	**794**	**1152**	**0.981**	**980**	0
						1155	1171	0.019		
UKL-3_21	OS-66653	Stick	−24.88	1510	25	**1334**	**1419**	**0.893**	**1388**	21
						1463	1512	0.107		
UKL-3_87-88	OS-66654	Stick	−24.04	2430	25	**2354**	**2504**	**0.758**	**2451**	87
						2528	2538	0.009		
						2594	2614	0.045		
						2637	2696	0.187		
UKL-3_185	OS-66655	Cone	−22.68	4410	30	**4866**	**5054**	**0.946**	**4981**	185
						5189	5214	0.043		
						5226	5232	0.004		
						5249	5258	0.007		
UKL-3_277	OS-66656	Wood	−28.61	6370	35	**7249**	**7418**	**1.000**	**7304**	277
UKL-3_315	OS-66594	Wood	−22.4	6780	40	**7577**	**7678**	**1.000**	**7629**	315

[a] Boldface highlights most-probable age range.
[b] Adjusted by 1090 ^{14}C yrs in depth-age model.
[c] Equivalent depth in Core UKL-1.

Valley is not known, so an age of 15,000 BP was used in the model based on results of a study in Flathead Lake to the west of GNP (Hofmann and Hendrix, 2010) and recently acquired [10]Be surface-exposure ages for boulders on the terminal moraine of Cut Bank Creek, along the east side of GNP ~50 km southeast of Cosley Lake (Laabs, unpublished).

Depth-age models were constructed for all five cores using the radiocarbon results and the other information germane to stratigraphic age. Appropriate ages were inferred for the sediment–water interface of each core (−57 BP for the cores from Upper Kintla Lake, and −60 BP for the others). Cubic spline functions were fit to the median probability for each calibrated radiocarbon age. This approach permitted estimation of ages for samples at depths between control points, while avoiding sharp changes in sedimentation rate. Given the strong similarities between cores UKL-1 and UKL-2, ^{14}C ages for the UKL-2 core were projected onto the UKL-1 record (which penetrated to a deeper stratigraphic depth) by wiggle-matching the LOI records. This combined set of ^{14}C ages, along with the ^{210}Pb results, was used in developing the depth-age model for the UKL-1 record.

Two ^{14}C ages were ignored in construction of these models. Sample UKL-1_39 (145 ± 30 ^{14}C yrs BP) failed to match the well-constrained ^{210}Pb decay curve that overlaps with this depth. Similarly, sample Cosley_192 yielded an age (9730 ± 50 ^{14}C yrs BP) incompatible with the age of the Mazama tephra layer ~15 cm higher. It is assumed that the organic fragments that yielded these results were buried temporarily in the watershed before being transported to the lake at a later date.

The depth-age models resulting from this approach are presented in Fig. 2. Using these models, core UKL-1 covers ~1000 years. The Cracker Lake core covers ~2000 years. The core from Harrison Lake extends for nearly 4000 years. Core UKL-3 bottoms in the Mazama tephra (7630 BP), and the core from Cosley Lake extend through the Mazama and back to the latest Pleistocene. Sedimentation rates range from 0.4 to 24.4 mm yr^{-1}, and sampling intervals vary from 0.4 to ~140 yrs (Table 1). Mean sedimentation rates are highest (3.4 mm/yr) at the site of UKL-1, immediately below the inflow from the Agassiz Glacier. The deep-water core from this same lake (UKL-3) exhibited a much lower average sedimentation rate of 0.5 mm/yr, similar to the coring site in Cosley Lake (0.3 mm/yr). The cores from Cracker and Harrison Lakes had similar, intermediate, rates (~1.5 mm/yr, Table 1).

3.4. Time-series

The sedimentary proxy time-series generated for the five records are presented in Fig. 3 through 7, while modern and period-of-record mean values are presented in Table 3. The shortest record, UKL-1, features a light-colored unit rich in very fine (VF) silt that accumulated before 900 BP, overlain by a darker, sandy layer with high MS values (Fig. 3). Values of bSi flux are generally low throughout (<10 mg/cm^2/yr). Values of CaCO$_3$ flux are variable, reaching progressively higher peaks culminating with values in excess of 75 mg/cm^2/yr ca AD 1920. Overall, intervals of high CaCO$_3$ flux are synchronous with high L* values (lighter colors), increases in BD and the abundance of VF silt, decreases in bSi flux, and low to moderate OM (Fig. 3).

The core from Cracker Lake bottomed in a dense, red (high a*) layer with elevated MS values that accumulated before 2000 BP (Fig. 4). Above this level most proxies exhibit fairly stable behavior, except for an interval centered on 1400 BP when the sedimentation rate increased. Because this interval is associated with an increase in median GS and abundance of VF sand, it likely reflects enhanced delivery of sediment to the coring site by mass wasting. An increased abundance of pebbles noted in this section of the core is consistent with this interpretation. Flux of CaCO$_3$ into Cracker Lake, rose over the last few centuries, reaching peak values of nearly 100 mg/cm^2/yr ca AD 1850, coincident with low values of bSi flux and high values of MAR and VF silt (Fig. 4).

The record from Harrison Lake features millennial-scale oscillations in several proxies including BD, MAR, OM, and VF silt (Fig. 5). Values of bSi flux are relatively high (~5 mg/cm^2/yr) before 3500 BP, after which they are very low until the last century, except for an interval from 2000 to 1500 BP. Generally intervals of low bSi flux coincide with decreased MAR and median GS, increases in the amount of VF silt, and higher L* values (Fig. 5).

Modern values from the deep-water coring site in Upper Kintla Lake (UKL-3) are notably different than the surface sediment at the site of core UKL-1 (Table 3). Organic matter content, CaCO$_3$ flux, and abundance of VF silt are greater in the deep-water sediment, whereas bSi flux, MAR, median GS, and the abundance of VF sand are greater at the site of UKL-1 (Fig. 6). These differences, along with the strongly contrasting physical settings of the two sites (Fig. 1), rule out appending UKL-1 to the top of the UKL-3 record. The remainder of the UKL-3 record exhibits a steady decrease in median
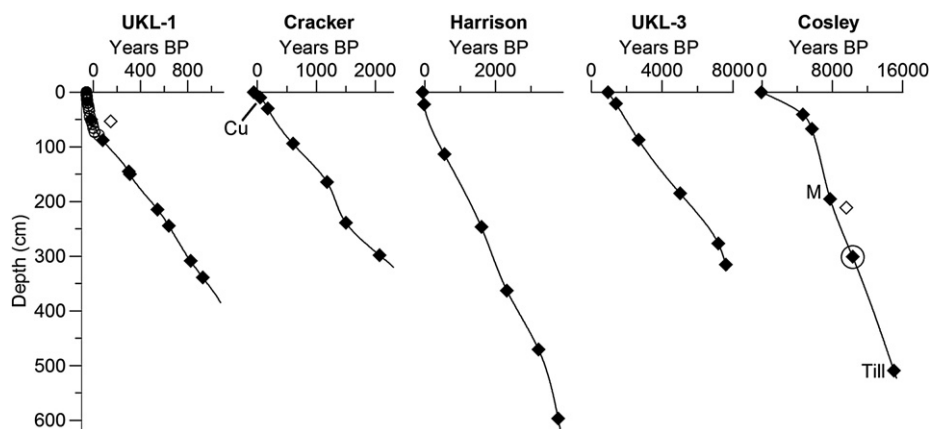

Fig. 2. Depth-age models for the cores included in this study. Models were generated by fitting cubic-spline curves to relevant age control. Overlapping open circles near the top of UKL-1 represent ^{210}Pb results. Solid black diamonds represent the maximum probability of each calibrated ^{14}C age (error ranges are too small to show at this scale, but are listed in Table 2). Open diamonds (two) represent ages ignored in the development of the age models. "Cu" marks the depth of a spike in copper abundance in the Cracker Lake core considered to reflect mining efforts in AD 1901. "M" represents the Mazama tephra. The circled age in the Cosley Lake record was adjusted 1090 ^{14}C yrs because of a potential hard water effect. "Till" denotes the diamicton encountered at the base of the Cosley Lake record, which was assigned an age of 15,000 BP given other evidence for the timing of deglaciation in this region. See text for details.
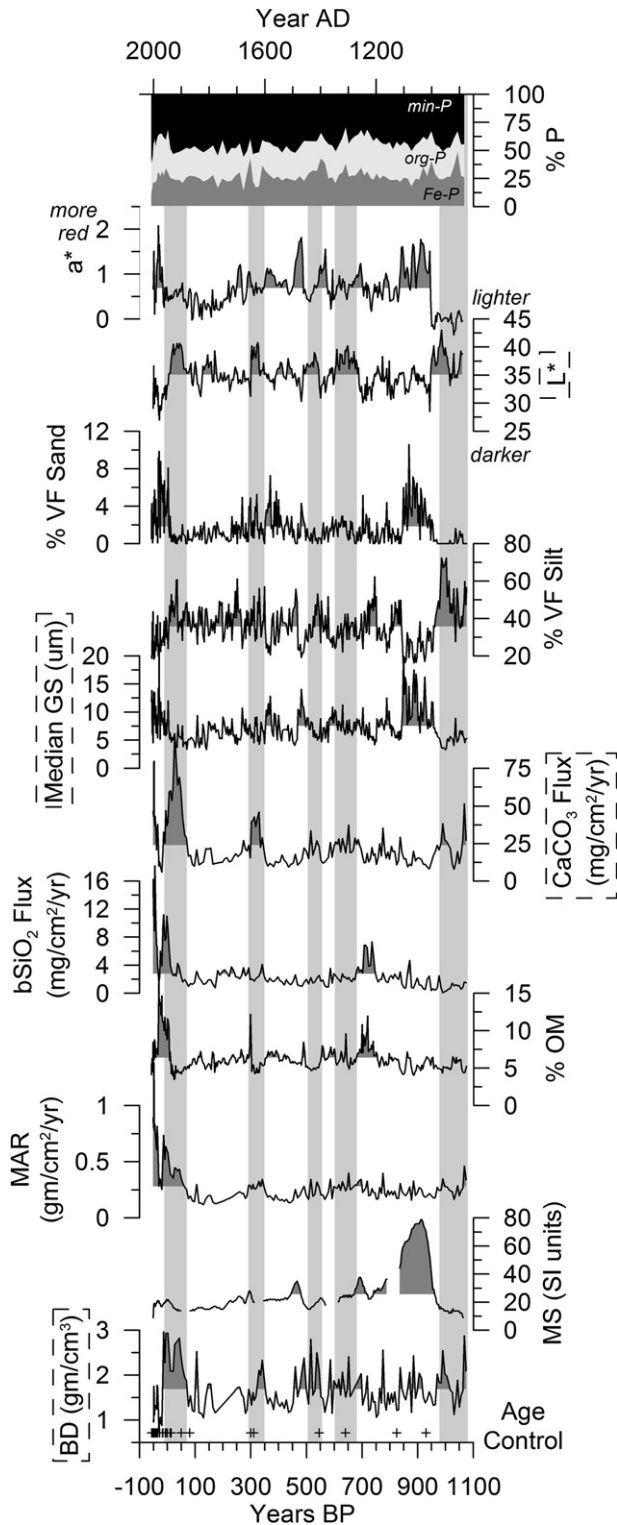
Fig. 3. Multi-proxy results for Core UKL-1. Small crosses denote locations of age control shown in Fig. 2. Bulk density (BD), magnetic susceptibility (MS), mass accumulation rate (MAR), organic matter content (% OM), biogenic silica (bSi) and carbonate (CaCO₃) flux, median grain size (GS), abundance of very fine (VF) silt and sand, the color values L* and a*, and the fractionation of phosphorus into iron-bound (Fe−P), organic (org-P), and mineral (min-P) are presented on a common timescale (years BP at bottom, years AD at top). Curves are filled relative to their mean values. Dashed boxes outline the time series considered most critical in identifying episodes of enhanced glacial rock flour delivery. Vertical gray bars highlight intervals in which the majority of proxies shift in directions consistent with elevated rock flour influx.

GS before ∼4000 BP, coinciding with a prominent increase in the abundance of VF silt (Fig. 6). Values of BD, MAR, OM, CaCO₃ flux, L*, and a* exhibit synchronous oscillations, with dense, light-colored sediment rich in CaCO₃ generally corresponding to low values of bSi flux.

The long record from Cosley Lake documents major shifts in the lacustrine environment associated with a long-term decrease in MAR (Fig. 7). A thick sequence of fine sediment overlies the basal diamicton that accumulated in the latest Pleistocene. This fine sediment exhibits high MS, CaCO₃ flux, and VF silt values, with undetectable bSi and very low OM content. Around the Pleistocene−Holocene transition the sediment gradually shifted to lower BD, CaCO₃ flux, and VF silt values, although OM remained low and bSi remained undetectable. This situation changed at the time of the Mazama tephra; above the tephra layer the sediment color changes abruptly, along with a dramatic increase in the abundance of VF sand and OM. Values of bSi flux also increase above the tephra layer, but this could be a result of glass shards dissolving in the sequential extraction and artificially inflating the apparent bSi values. Median GS remains high until ∼2000 BP, at which time there is a sustained drop in the abundance of VF sand (Fig. 7). Overall the modern sediment in Cosley Lake was notably different than that recovered from the other lakes; values of OM, median GS, and VF sand are the highest encountered in this study (Table 3).

4. Discussion

4.1. Interpretive strategy

Many studies have demonstrated that changes in glacier behavior are recorded in downstream lake sediment archives (e.g. Karlén, 1981; Leonard and Reasoner, 1999; Nesje, 2009). The fundamental explanation is that larger glaciers, which cover a greater area with thicker, more erosive ice, are generally more effective at generating fine-grained rock flour through bedrock erosion by subglacial sliding (Leonard, 1997). Delivery of this material to downstream lakes changes sediment characteristics in predictable ways. For example, bulk density and the abundance of (very) fine silt increase as a direct result of enhanced rock flour influx, whereas the abundance of biogenic silica and organic matter decrease. These latter changes may reflect dilution of these sedimentary components by the increased abundance of fine clastic material, or actual suppression of primary productivity in the lake due to reduced water temperature and clarity (e.g. Nesje et al., 2001; Kaplan et al., 2002; Nussbaumer et al., 2011).

Consideration of these causal relationships supports an interpretive framework for how the proxies investigated in this study would record changes in upstream ice extent. Given the proximity of the lakes to upstream glaciers (Fig. 1, Table 1), and their direct connection by perennial, topographically confined rivers, increases in BD, MAR, and VF silt coinciding with decreases in OM, bSi flux, and median GS likely indicate increased rock flour delivery. Simultaneous increases in the abundance of CaCO₃ flux and L* in Cosley, Cracker, and Upper Kintla Lakes would also be consistent with greater rock flour influx because the cirques upstream from these lakes are eroded into limestone bedrock (Whipple, 1992). The records of P fractionation developed for Upper Kintla Lake would be expected to show greater abundance of mP, and possibly Fe−P from soil erosion, at these times, with a corresponding decrease in the abundance of org-P (Filippelli et al., 2006). Finally, given the low abundance of iron-bearing lithologies upstream of the studied lakes, MS should be low during times of enhanced rock flour delivery. In contrast, high values of MS could signify deposition of volcanic tephra or slope processes that delivered iron-bearing lithologies directly to the lake.

Table 3
Modern and period-of-record mean proxy values.

Proxy		UKL-1		UKL-3		Cracker		Cosley		Harrison	
		Modern	Mean	Modern	Mean	Modern	Mean	Modern	Mean	Modern	Mean
Water	%	–	4.2	67.5	45.4	35.7	34.3	68.7	40.6	77.8	41.1
OM	%	4.9	6.4	6.7	6.0	3.8	3.6	9.5	4.0	5.8	4.1
Carbonate	mg/cm^2/yr	0.05	0.02	0.64	1.19	0.03	28.57	0.03	3.36	28.04	4.90
bSi	mg/cm^2/yr	16.29	3.07	0.24	0.45	0.03	0.25	0.10	1.03	7.45	2.13
MAR	gm/cm^2/yr	0.89	0.31	0.03	0.04	0.12	0.23	0.001	0.02	0.60	0.12
Median GS	um	12.5	7.5	5.7	8.7	3.6	4.2	13.9	7.8	6.0	5.1
VF silt	%	19.4	35.8	31.8	36.3	59.3	52.4	9.0	17.8	42.5	53.1
VF sand	%	3.7	1.8	3.1	2.4	0.0	0.2	19.2	5.8	0.3	0.1
L*	–	–	35.1	–	37.9	–	45.1	–	46.9	–	42.3
a*	–	–	0.7	–	0.3	–	1.7	–	2.4	–	2.8
b*	–	–	5.2	–	5.1	–	5.1	–	6.1	–	6.9

An additional consideration in the interpretation of these records is the phase of each glacial cycle most likely to be recorded in the lake sediment. A maximum rate of sediment production is likely achieved during the peak of a given glacier advance, when the erosive capability of the ice is greatest (Leonard, 1997). However, this sediment may not be immediately delivered to downstream lakes if it is first stored in the subglacial or englacial environment. Support for this concept comes from studies of varved records, which demonstrate that the greatest rate of sediment output from a glacier occurs during transitional phases, particularly intervals of rapid retreat (Leonard, 1997; Menounos and Clague, 2008). This potential lag between the peak of rock flour production and maximum values of rock flour delivery to downstream lakes is further influenced by the filtering role played by the resolution of each record. In ice-proximal, high-resolution records, like those from Cracker Lake and core UKL-1, where each cm corresponds to <10 yrs on average, it is possible that individual sub-decadal-scale events are recorded. In these records, even after accounting for the blurring effects of bioturbation, discrete spikes in the abundance of carbonate-rich, VF silt likely reflect individual episodes of extensive glacier retreat. In contrast, the lower resolution records from Harrison and Cosley Lakes (which were analyzed primarily at 2-cm intervals) and core UKL-3 are unlikely to record individual episodes of glacier retreat. Instead, intervals of elevated rock flour in these cores likely record centennial-scale episodes of increased glacier activity in which multiple advance–retreat cycles are blended together by the time-averaging processes of temporary sediment storage and bioturbation. This distinction is important when considering the set of records from GNP, especially given recent recognition that past intervals of Neoglacial activity were likely as complicated on sub-centennial timescales as the generally better-dated Little Ice Age (Clague et al., 2009). The different resolutions offered by the entire collection of cores from GNP (Table 1), therefore, offer the complementary potential for detecting short-term, rapid events (interpreted as specific retreat phases) during the past millennium, as well as prolonged intervals of heightened glacier activity earlier in the Holocene.

Validation of the logic behind this interpretative framework is provided by comparison of documented retreat rates of the Agassiz Glacier and the record of CaCO$_3$ flux in core UKL-1 adjacent to Agassiz River inflow to Upper Kintla Lake (Fig. 8). Tree-ring data collected inside the LIA terminal moraine of the Agassiz Glacier (Carrara and McGimsey, 1981) indicate that retreat began there ca AD 1860, but remained slow (~5 m/yr) until the early part of the 20th Century (Fig. 8). Rates then increased dramatically to maximum values in excess of 100 m/yr ca AD 1930, as the glacier retreated up a series of ledges that dip steeply down-valley. Measured values of CaCO$_3$ flux in core UKL-1 parallel this trend,

beginning to rise at the onset of ice retreat, reaching a maximum nearly synchronous with the fastest ice retreat rates, and decreasing as retreat rates tapered in the 20th Century (Fig. 8). A late rise in CaCO$_3$ flux also corresponds with a slight acceleration of retreat rate during the last few decades. Flux of CaCO$_3$ to Upper Kintla Lake, therefore, is strongly linked to retreat of the Agassiz Glacier, corroborating prior studies that link short-term maximum sediment loads with transitional glacier behavior (e.g. Leonard, 1997). This connection supports the use of rock flour as a proxy for ice retreat in the high resolution records (UKL-1 and Cracker Lake) as well as the use of rock flour as a proxy for overall increases in glacier area and activity in the records with lower resolution (Harrison, UKL-3, and Cosley Lake).

Given this interpretive framework, the five records from GNP were evaluated for evidence of synchronous proxy changes suggesting increases in the delivery of rock flour. As is the case in most paleolimnological investigations, no single proxy is unequivocally diagnostic of upstream glacier activity in all five records. However, some proxies track upstream glaciers with higher fidelity given the specifics of each glacier-lake system. In this study, the abundance of CaCO$_3$ is considered most revealing in Upper Kintla and Cracker Lakes where upstream glaciers rest directly on extensive areas of limestone bedrock. Median GS and abundance of VF silt are of primary significance in the records from Harrison Lake (where upstream limestone is minimal) and Cosley Lake (where upstream limestone is present, but the overall size of individual glaciers is small compared with the extent of the watershed). Values of BD and L* are also useful, for instance in core UKL-1, which is dominated by light-colored clastic sediment. These proxies, which are highlighted with dashed-line boxes in Figs. 3–7, were inspected as a first step toward unlocking the Neoglacial records contained within these cores. Intervals of above mean CaCO$_3$ flux and VF silt abundance, and median GS below mean values, that are synchronous with shifts in other proxies matching the interpretive framework, are highlighted with gray bars in Figs. 3–7. Fig. 9 presents a composite view of this Neoglacial history in which the complementary, nested nature of the five records is obvious. A summation is also provided illustrating the percentage of records exhibiting elevated rock flour abundance with a 10-yr time step (Fig. 9).

4.2. History of Neoglaciation

4.2.1. Last millennium

All of the records except for Cosley Lake contain evidence for glacier advances during the last millennium (Fig. 9), corresponding with the Little Ice Age (Grove, 2004), which is strongly expressed globally (Davis et al., 2009). Historical photography, eyewitness observations, and tree-ring records all document greater-than-
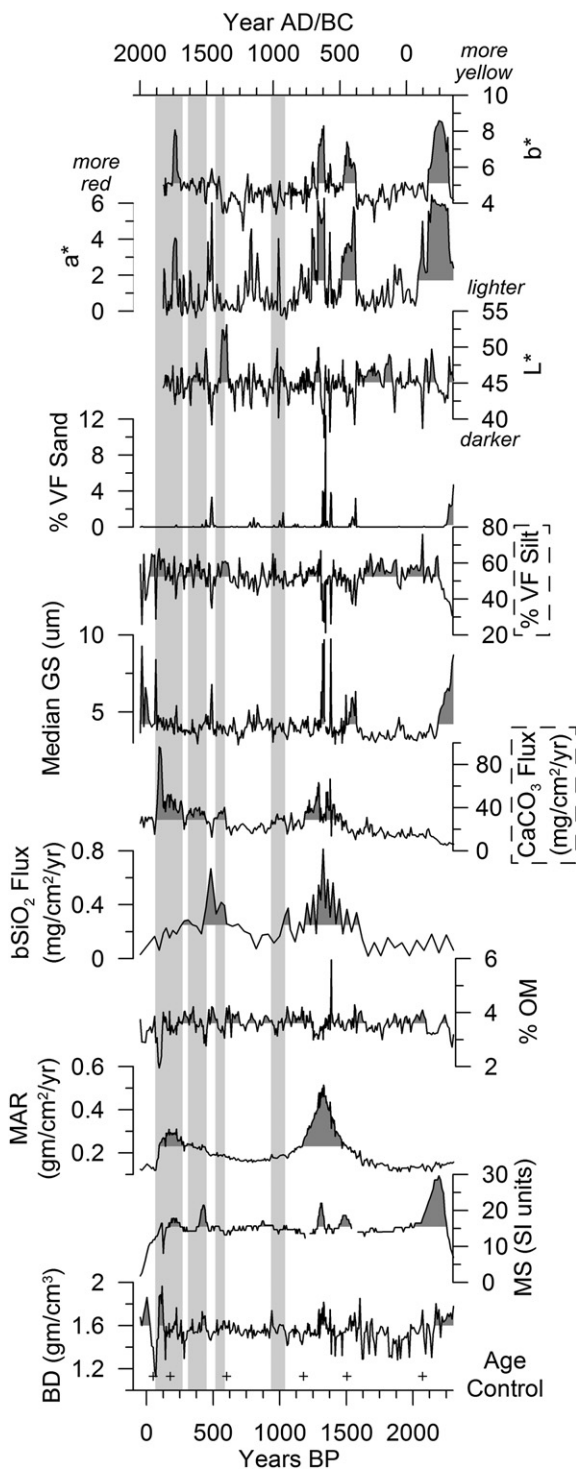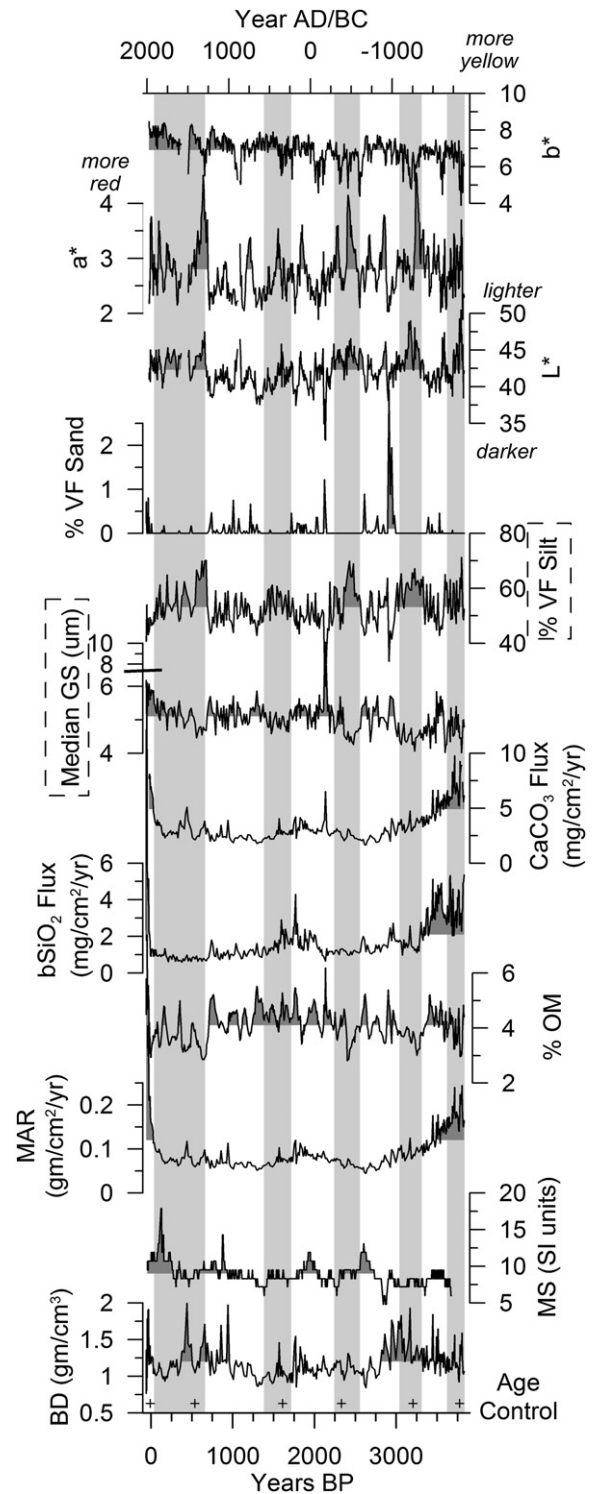
Fig. 4. Multi-proxy results for Cracker Lake. Small crosses denote locations of age control shown in Fig. 2. Bulk density (BD), magnetic susceptibility (MS), mass accumulation rate (MAR), organic matter content (%OM), biogenic silica (bSi) and carbonate (CaCO₃) flux, median grain size (GS), abundance of very fine (VF) silt and sand, the color values L*, a*, and b* are presented on a common timescale (years BP at bottom, years AD at top). Curves are filled relative to their mean values. Dashed boxes outline the time series considered most critical in identifying episodes of enhanced glacial rock flour delivery. Vertical gray bars highlight intervals in which the majority of proxies shift in directions consistent with elevated rock flour influx.
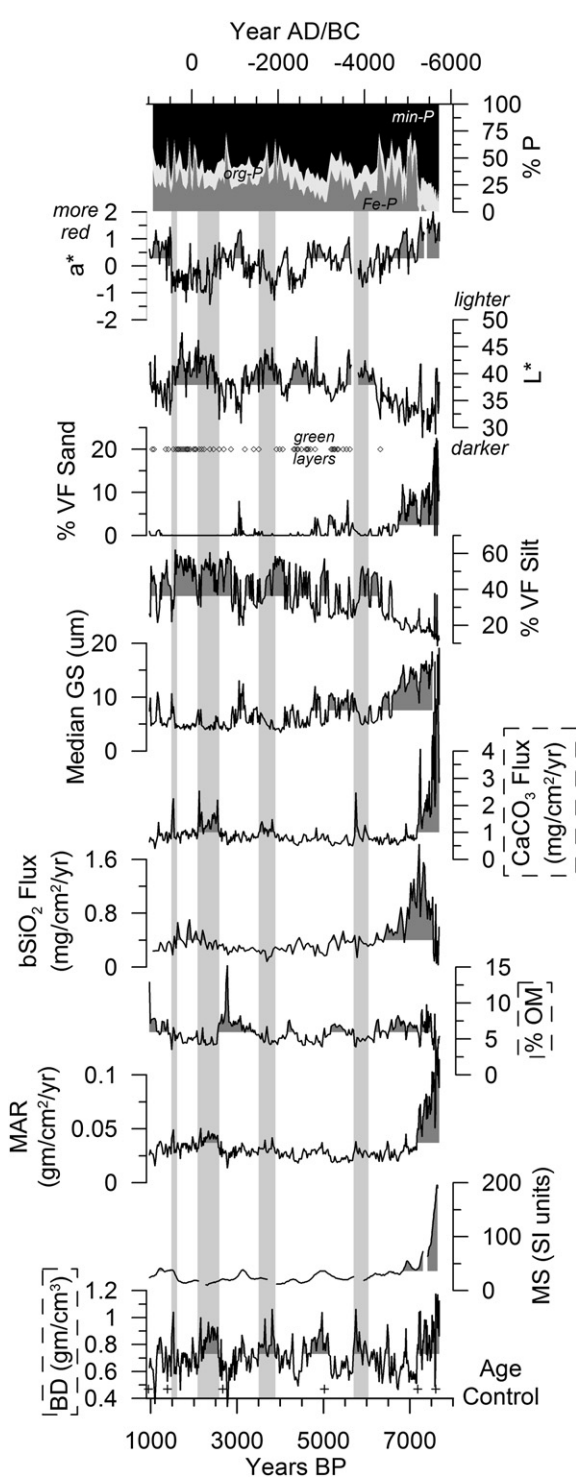
Fig. 5. Multi-proxy results for Harrison Lake. Small crosses denote locations of age control shown in Fig. 2. Bulk density (BD), magnetic susceptibility (MS), mass accumulation rate (MAR), organic matter content (%OM), biogenic silica (bSi) and carbonate (CaCO₃) flux, median grain size (GS), abundance of very fine (VF) silt and sand, the color values L*, a*, and b* are presented on a common timescale (years BP at bottom, years AD at top). Curves are filled relative to their mean values. Dashed boxes outline the time series considered most critical in identifying episodes of enhanced glacial rock flour delivery. Vertical gray bars highlight intervals in which the majority of proxies shift in directions consistent with elevated rock flour influx.
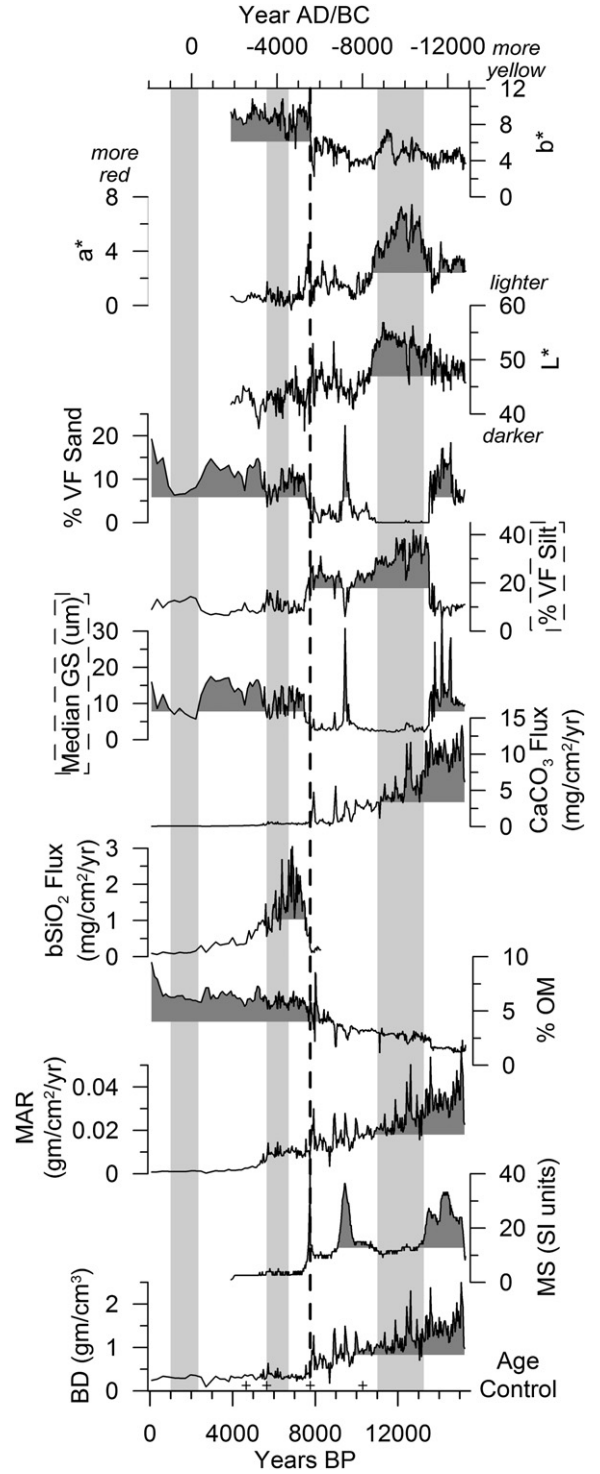
Fig. 6. Multi-proxy results for Core UKL-3. Small crosses denote locations of age control shown in Fig. 2. Bulk density (BD), magnetic susceptibility (MS), mass accumulation rate (MAR), organic matter content (% OM), biogenic silica (bSi) and carbonate ($CaCO_3$) flux, median grain size (GS), abundance of very fine (VF) silt and sand, the color values L* and a*, and the fractionation of phosphorus into iron-bound (Fe–P), organic (org-P), and mineral (min-P) are presented on a common timescale (years BP at bottom, years AD at top). Curves are filled relative to their mean values. Diamonds designate the inferred ages of discrete <1-cm thick green layers rich in chips of argillite derived from the surrounding hillslopes. Dashed boxes outline the time series considered most critical in identifying episodes of enhanced glacial rock flour delivery. Vertical gray bars highlight intervals in which the majority of proxies shift in directions consistent with elevated rock flour influx.
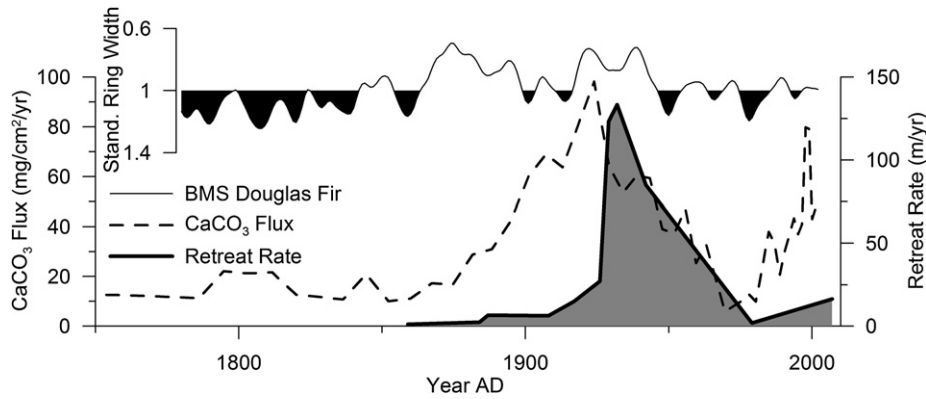
Fig. 7. Multi-proxy results for Cosley Lake. Small crosses denote locations of age control shown in Fig. 2. Bulk density (BD), magnetic susceptibility (MS), mass accumulation rate (MAR), organic matter content (% OM), biogenic silica (bSi) and carbonate ($CaCO_3$) flux, median grain size (GS), abundance of very fine (VF) silt and sand, the color values L*, a*, and b* are presented on a common timescale (years BP at bottom, years AD at top). MS and color values could not be determined for the unconsolidated sediment retrieved from the surface core from this lake. Curves are filled relative to their mean values. The vertical dashed line marks the position of the Mazama tephra, which was removed from the time series because it represents an instantaneous event. bSi was undetectable below the Mazama tephra. Dashed boxes outline the time series considered most critical in identifying episodes of enhanced glacial rock flour delivery. Vertical gray bars highlight intervals in which the majority of proxies shift in directions consistent with elevated rock flour influx.

Fig. 8. Relationship between climate, retreat of the Agassiz Glacier, and flux of carbonate in core UKL-1 from AD 1750 to the present. Dashed line shows CaCO$_3$ flux in mg/cm^2/yr. Filled gray line illustrates the reconstructed retreat rate of the Agassiz Glacier from its LIA terminal moraine, calculated from dating of trees in the glacier forefield (Carrara and McGimsey, 1981). Carbonate flux began to rise at the onset of ice retreat, and reached a peak nearly synchronous with the maximum reconstructed retreat rates ca AD 1930. Filled black line presents a tree-ring compilation (BMS Douglas Fir) sensitive to summer drought collected in the vicinity of the Agassiz Glacier (Pederson et al., 2004). Black fill (note reversed scale) denotes wetter, cooler conditions that were responsible for advance of the Agassiz Glacier to its LIA maximum position. Retreat began with the switch to below-normal precipitation.

modern ice extents in GNP during the 19th Century, at the end of this interval (e.g. Carrara and McGimsey, 1981; Carrara, 1987). Retreat from this ice extent maximum is recorded in Cracker Lake and core UKL-1, the two most ice-proximal cores, as record-high values of CaCO$_3$ flux corresponding with high BD and L*, and low bSi flux signifying elevated rock flour influx (Figs. 3 and 4). In both lakes this most recent peak in CaCO$_3$ flux is the largest on record, indicating that retreat from the LIA maximum was the most dramatic in the period represented by the cores. The timing of this peak, however, is different in the two records, occurring ca AD 1855 in Cracker Lake, and ca AD 1920 in core UKL-1 (Fig. 10). It is possible that retreat was actually synchronous and that the differences in timing are a result of error in the age models. However, the CaCO$_3$ peak in the Cracker Lake record (16 cm depth) is closely constrained by the spike in Cu abundance (11 cm) tied to historically documented mining activity. Similarly, the CaCO$_3$ peak in the UKL-1 record (70 cm depth) is well-constrained by the ^{210}Pb results that extend to a depth of 80 cm. Thus, it is more likely that the difference in timing of peak CaCO$_3$ flux is real, probably reflecting contrasting glacier response time. Reconstructions based on preserved

moraines indicate that the Agassiz Glacier covered about eight times the area of the Siyeh Glacier at its maximum LIA extent (Key et al., 2002). Elevations of lateral moraine remnants above modern valley floors also indicate that the Agassiz Glacier was more than twice as thick as the Siyeh Glacier during the peak of the LIA. Both of these differences would have made the Agassiz Glacier more resilient in the face of a changing climate at the end of the LIA.

Older peaks of CaCO$_3$ flux reveal that the culminating LIA advance was preceded by other advance/retreat cycles (Fig. 10), supporting the conclusion that the LIA was a complex interval in which alpine glaciers oscillated in a generally expanded state (Clague et al., 2009). Core UKL-1, for instance, records a major peak in CaCO$_3$ flux in the early 17th Century, as well as generally elevated values ca AD 1300. Values in Cracker Lake, which averaged 50% of their LIA-retreat maximum during the LIA advance phase were also high from AD 1500–1600, and ca AD 1400. Once again, offsets in the timing of these intervals likely reflect contrasting glacier response times, but it is clear that the glaciers upstream from these lakes advanced and retreated numerous times in the past millennium (Fig. 9).
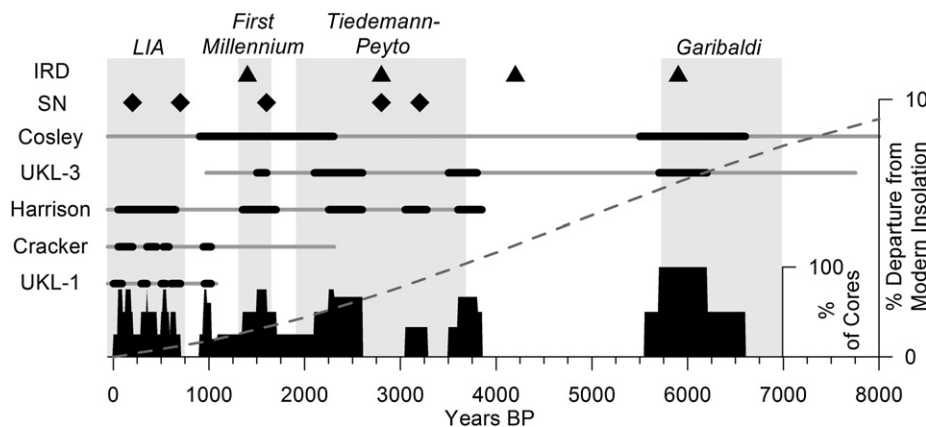

Fig. 9. Summary of the Neoglacial record developed for Glacier National Park. Black bars denote intervals of enhanced rock flour deposition, while gray bars represent the entire length of each record (note that the Cosley Lake record was truncated for clarity). Diamonds designate intervals of glacier expansion determined from lacustrine evidence in the Sierra Nevada (SN) (Bowerman and Clark, 2011). Triangles identify peaks of ice-rafted debris (IRD) in the North Atlantic (Bond et al., 1997). Vertical gray bars highlight the Little Ice Age (Grove, 2004), First Millennium (Reyes et al., 2006), Tiedemann-Peyto (Clague et al., 2009), and Garibaldi Neoglacial phases (Clague et al., 2009). Dashed line illustrates decreasing summer insolation (as a percentage of modern) over the past 8000 years (Berger, 1978). Summation at the bottom shows the percentage of records illustrating evidence for enhanced rock flour deposition determined with a 10-yr time step.
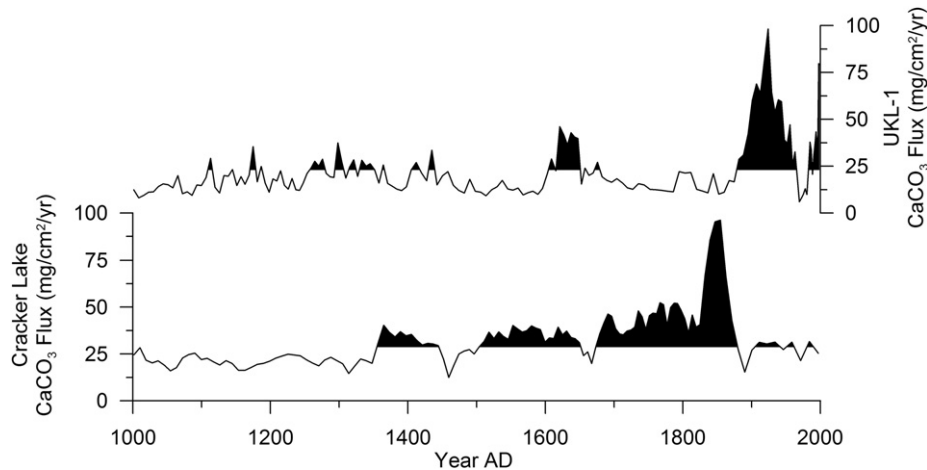
Fig. 10. Records of CaCO$_3$ flux to Cracker Lake (bottom) and Upper Kintla Lake (top) for the past millennium. Offset in timing of the post-LIA peak likely reflects differences in glacier response time driven by the larger size of the Agassiz Glacier above Upper Kintla Lake. Older episodes of elevated CaCO$_3$ flux reveal that the LIA contained multiple advance/retreat cycles.

The longer record from Harrison Lake also contains signals of glacier activity in the late Holocene, although as explained above, intervals of elevated rock flour in this lower-resolution core are not interpreted as evidence of individual glacier retreat events. Instead, these intervals are considered to reflect an overall increase in time-averaged glacier area and, possibly, more frequent fluctuations of larger glaciers. The lack of carbonate bedrock in the vicinity of the Harrison Glacier also requires reliance on other proxies when interpreting the record from Harrison Lake. Accordingly, low bSi flux and OM values, combined with elevated VF silt abundance, indicate that the Harrison Glacier was more extensive from AD 1300 to the present, which corresponds with the LIA signal seen in Cracker Lake and core UKL-1 (Fig. 5).

The core from Cosley Lake lacks a clear signal of glacier activity in the past millennium (Fig. 9). Both median GS and the abundance of VF sand in the long core from this lake increase in the last few centuries (Fig. 7), and this change was also noted in three surface cores taken along the axis of the lake basin (Fig. 1D). Given the depth-age model and interpretive framework, this increase in sediment size would suggest a decrease in glacierized area at the same time that glaciers elsewhere in GNP were advancing toward their LIA maximum positions. However, the depth-age model in the upper section of the Cosley core is not well constrained (Figs. 2 and 7) and it is possible that the coarsening of the sediment, which is confined to the uppermost few cm, occurred more recently than the model suggests, perhaps following the LIA. Alternatively, changes in the upstream surface connection to Glenns Lake, through which sediment and water must move before reaching Cosley, may have impacted the coarseness of the near-surface sediment.

4.2.2. Pre-last millennium

The longer records from Cosley, Harrison, and Upper Kintla Lakes reveal evidence for multiple pulses of Neoglacial activity earlier in the Holocene. For example, core UKL-3 records enhanced rock flour deposition from 1500 to 1600 BP, which falls within longer intervals of low median GS in the Cosley Lake and Harrison Lake records (Fig. 9). This timing aligns well with an episode of glacier expansion in the Sierra Nevada ca 1600 BP (Bowerman and Clark, 2011), and overlaps with glacial advances during the first millennium in the Pacific Coast Ranges of Alaska and British Columbia (Denton and Karlén, 1973; Reyes et al., 2006), referred to as the First Millennium Advance (Menounos et al., 2009).

Farther back in time, both the Harrison and Agassiz Glaciers were enlarged and active between 2600 and ∼2100 BP, which overlaps with a prolonged interval of low median GS values in Cosley Lake that began ca 2300 BP (Fig. 9). Harrison Glacier was also enlarged and active from 3600 to 3850 and 3050 to 3300 BP (Fig. 9). The older of these two intervals matches proxy shifts in core UKL-3 from 3500 to 3800 BP that are consistent with an enlarged Agassiz Glacier (Figs. 6 and 9). Elsewhere in GNP, pulses of elevated abundance of detrital dolomite in a core from Swiftcurrent Lake during this same interval were considered evidence of short-term retreats of an enlarged Grinnell Glacier (MacGregor et al., 2011). Collectively, therefore, there is strong evidence that glaciers in GNP were enlarged and active between ∼2000 and 4000 BP. This timing corresponds with the well-documented Tiedemann-Peyto advances in western Canada (Ryder and Thomson, 1986; Luckman et al., 1993; Koch et al., 2007; Clague et al., 2009; Menounos et al., 2009), implicating a regional climate forcing that promoted positive glacier mass balance at this time. Lacustrine evidence for glacier expansion during this interval has also been reported from the Sierra Nevada (Bowerman and Clark, 2011), and this interval encompasses a global episode of cooler climate identified in a compilation of over 40 temperature-sensitive paleoclimate records (Wanner et al., 2011).

No evidence is seen in the records for enhanced rock flour deposition from 4000 to 5500 BP (Fig. 9), an interval covered only by the record from Cosley Lake and core UKL-3. In Upper Kintla Lake, values of CaCO$_3$ flux and MAR are consistently low, suggesting minimal deposition of rock flour (Fig. 6). In Cosley Lake values of VF silt remain near record-low levels, also suggesting low rock flour input (Fig. 7). This interval corresponds to a quiescent period in the cumulative Neoglacial history for western Canada (Clague et al., 2009). Some evidence has been reported for local glacier advances during this time (e.g. Menounos et al., 2008), but the small number of studies prohibits evaluation of the potential regional significance of these reports.

Both Cosley Lake and core UKL-3 contain strong evidence for expanded glaciers earlier in the Holocene (Fig. 9). In core UKL-3, OM decreases while CaCO$_3$ flux, VF silt, BD, and L* increase from 5700 to 6200 BP (Fig. 6). In Cosley Lake values of VF silt are relatively high (for the post-Mazama period) from 5500 to 6600 BP, coinciding with a drop in VF sand and a minor rise in the abundance of CaCO$_3$ (Fig. 7). Together these shifts indicate that the Agassiz Glacier, and glaciers in the headwaters of the Mokowanis River,

expanded ca 6500 BP. These glaciers may not have sustained an advanced position over the duration of each of these intervals, but the proxy shifts are consistent with larger volumes of meltwater and increased glacial erosion. This timing overlaps directly with the Garibaldi Glaciation in western Canada from 5600 to 6900 BP (e.g. Ryder and Thomson, 1986; Koch et al., 2007; Clague et al., 2009), once again implicating a regional climatic driver. Glacier advance ca 6500 BP is also the oldest Neoglacial event recorded in this suite of cores and may indicate the return of cirque glaciers to GNP after the Hypsithermal interval (Matthes, 1942).

Inspection of the proxy records from core UKL-3 reveals another interval from 7450 to 7750 BP that exhibits some hallmarks of increased clastic sedimentation, namely an increase in $CaCO_3$ flux and BD (Fig. 6). However, MS values are very high during this interval, L* is very low, and the sediment is coarser than at any other point in the record, all of which are inconsistent with increasing rock flour influx. An alternative explanation for these proxy trends is that this layer records deposition of the Mazama tephra and enhancement of slope processes, perhaps aided by intense precipitation. Previous studies have noted stratigraphic correspondence between tephra layers and debris flow deposits, and inferred that past Plinian eruptions spawned strong thunderstorms that initiated mass wasting events (Bell and House, 2007). In the case of GNP, the Mazama tephra in Upper Kintla Lake was intermixed with a layer of unusual coarseness, the ash layer in Swiftcurrent Lake was nearly 50-cm thick with ~25% clastic material (MacGregor et al., 2011), and the Mazama layer in Cosley Lake contained clastic material up to 1-cm in diameter, all of which are suggestive of enhanced mass wasting at the time of Mazama ash deposition.

Finally, the long record from Cosley Lake contains a suggestion that glaciers expanded upstream between 11,000 and 13,200 BP. Abundance of light-colored, VF silt is very high during this interval (Fig. 7), which is consistent with increased amounts of rock flour traveling down the Mokowanis River. Even with the limitations of the age model at this depth, this timing overlaps with the Younger Dryas (YD) chronozone in the North Atlantic region. Glaciers elsewhere in GNP also advanced at this time, as shown by lacustrine evidence from Otokomi Lake, 25 km south of Cosley (MacLeod et al., 2006), and by the presence of detrital dolomite in Swiftcurrent Lake that could be considered evidence of upstream glacier activity (MacGregor et al., 2011). Together these observations suggest that alpine glaciers in GNP, probably surviving remnants of the much larger glaciers that occupied this region during the Last Glacial Maximum, readvanced during the YD. Regionally, moraines of the Crowfoot advance dating to this time interval have been identified as evidence of YD-related impacts on the Canadian Rocky Mountains (Reasoner et al., 1994), and it is logical that these effects would have been manifest in GNP.

4.2.3. Climate drivers

The Neoglacial history inferred from the five cores in this study exhibits strong correspondence with other records developed for western North America. Although it would be an oversimplification to conclude that glaciers throughout this region behaved in phase on multi-decadal timescales (e.g. Clague et al., 2009), the general coherence between records spanning over 20° of latitude is strong evidence for unifying drivers of millennial- to centennial-scale climate change in this region during the Holocene.

The forcing responsible for Neoglacial fluctuations varies depending on the timescale. At the longest timescale, steadily decreasing summer insolation may be responsible for the apparent time-transgressive nature of the Neoglacial onset along a north-south transect of the North American Cordillera. Some glaciers in western Canada advanced in association with the 8.2 ka Event in

the early Holocene (Menounos et al., 2004). This compilation indicates that glaciers in GNP advanced as early as 6500 BP, similar to glaciers at an equivalent latitude on Mt. Baker in northern Washington (Osborn et al., 2012). Yet, farther south, Neoglaciation began in the Sierra Nevada as recently as 3200 BP (Bowerman and Clark, 2011), and extensive rock glacier activity in the central Colorado Rockies began ca 3000 BP (Refsnider and Brugger, 2007). This overall pattern may track the intersection of a cooling climate and conditions necessary for glacierization, while anomalies within this pattern could illuminate the effects of local and regional-scale climatic factors.

Over centennial to millennial timescales, studies have proposed that episodes of glacier expansion occur during times of reduced solar irradiance (e.g. Denton and Karlén, 1973; Koch et al., 2007). This relationship was solidified by identification of a link between ice-rafted debris (IRD) in the North Atlantic, and solar irradiance as tracked by the production of atmospheric cosmogenic nuclides (Bond et al., 2001). The IRD variability features a quasi-periodic cycle of ~1500 yrs, and has been connected to glacier fluctuations in Europe (Holzhauser et al., 2005; Matthews et al., 2005; Nussbaumer et al., 2011). Similar variability is seen in records of vegetation composition across North America (Viau et al., 2002), and it is notable that three of the last four peaks in IRD, at 1400, 2800, and 5900 BP (Bond et al., 1997) match times of inferred Neoglacial activity in GNP (Fig. 8), suggesting that solar variability might underlie the long-term waxing and waning of alpine glaciers in this region. On the other hand, recent studies integrating large numbers of Holocene paleoclimate records have documented a lack of clear cyclicity and considerable spatiotemporal variability within global patterns of climatic changes (Wanner et al., 2008, 2011), indicating that internal climate variability and feedback loops play a major role in controlling climatic conditions on sub-regional scales.

In modern climate records, summer temperature exerts a strong control over glacier behavior in GNP, modulated by winter precipitation, and significant correlations have been documented between 20th century glacier fluctuations, the Pacific Decadal Oscillation (PDO), and snowfall (Pederson et al., 2004). For example, tree-ring data from the vicinity of the Agassiz Glacier (Pederson et al., 2004) demonstrate that LIA maximum was driven by a multi-decadal stretch of wet winters and cool summers spanning the early 19th Century (Fig. 8). In Fig. 8 this interval ends ca AD 1850, synchronous with the onset of ice retreat and the rise in $CaCO_3$ flux in core UKL-1. A leveling-off of $CaCO_3$ flux ca AD 1900 corresponds with a short-term return to wetter, cooler summers, and a second stretch of increased summer drought coincides with maxima of glacier retreat and $CaCO_3$ flux values. Extrapolating to longer timescales, changes in precipitation patterns may have played a role in governing the increasing magnitude of Neoglacial fluctuations, as well as the timing of Holocene glacier fluctuations. Pollen data for a site within GNP (Pederson et al., 2006) indicate a shift to cooler, wetter conditions after 4000 BP, corresponding to the onset of the Tiedemann-Peyto interval and advances of (at least) the Agassiz and Harrison Glaciers (Fig. 9). Modeling results also reveal a progressive intensification of the El Niño/Southern Oscillation since the middle Holocene (Clement et al., 2000), which would have enhanced winter precipitation during negative phases of the PDO (McCabe et al., 2000), shown to correspond with increased snow depth in GNP (Selkowitz et al., 2002). Although PDO fluctuations are too rapid to be directly responsible for the multi-centennial intervals of glacier expansion noted in this study, the PDO may have played a role in pacing the higher frequency advance–retreat cycles that punctuated episodes of overall glacier expansion.

Overall, Neoglacial fluctuations in GNP are a complicated product of multi-decadal to centennial-scale changes in summer temperature and winter precipitation superimposed on a long-term trend of gradually decreasing summer insolation. Broad synchrony between Neoglacial records in western North America illustrates a regional footprint for these changes, and correspondence of the most extensive event (the LIA) with glacier fluctuations in Europe indicates that alpine glacial systems can operate in phase on a hemispheric scale. However, robust inter-regional synchrony is unlikely given the importance of regionally specific climate amplifiers (e.g. Schaefer et al., 2009).

5. Conclusions

Detailed multi-proxy study of five sediment cores from four lakes supports interpretations about the history of Neoglaciation in Glacier National Park (GNP). Major conclusions of this work include:

1) Retreat from the Little Ice Age maximum advance (post-AD 1850) is the most dramatic episode of ice retreat in at least the last 1000 years.
2) The Little Ice Age maximum advance was just the most recent in a series of advance/retreat cycles during the past several millennia.
3) Glaciers in GNP advanced during the First Millennium (1300—1600 BP), Tiedemann-Peyto (1900—3700 BP) and Garibaldi (5700—6900 BP) phases reported from western Canada, implicating a regional climatic forcing for Neoglacial advances.
4) The onset of Neoglaciation occurred ca 6500 BP, which is earlier than reported for locations farther south in the Rocky Mountains and Sierra Nevada.
5) Glaciers in the headwaters of the Mokowanis River may have advanced during the Younger Dryas, corresponding to the formation of the Crowfoot moraines in western Canada.

Acknowledgments

References

Appenzeller, T., 2007. The Big Thaw. National Geographic June, 56—71.
Barclay, D.J., Wiles, G.C., Calkin, P.E., 2009. Holocene glacier fluctuations in Alaska. Quaternary Science Reviews 28, 2034—2048.
Bell, J.W., House, P.K., 2007. Did Plinian eruptions in California lead to debris flows in Nevada? An intriguing stratigraphic connection. Geology 35, 219—222.
Berger, A.L., 1978. Long-term variations of caloric insolation resulting from the Earth's orbital elements. Quaternary Research 9, 139—167.
Bond, G., Showers, W., Cheseby, M., Lotti, R., Almasi, P., Demenocal, P., Priore, P., Cullen, H., Hajdas, I., Bonani, G., 1997. A pervasive millennial-scale cycle in North Atlantic Holocene and glacial climates. Science 278, 1257—1266.
Bond, G., Kromer, B., Beer, J., Muscheler, R., Evans, M.N., Showers, W., Hoffmann, S., 2001. Persistent solar influence on north Atlantic climate during the Holocene. Science 294, 2130—2136.
Bowerman, N.D., Clark, D.H., 2011. Holocene glaciation of the central Sierra Nevada, California. Quaternary Science Reviews 30, 1067—1085.
Brown, J., Harper, J., Humphrey, N., 2010. Cirque glacier sensitivity to 21st century warming; Sperry Glacier, Rocky Mountains, USA. Global and Planetary Change 74, 91—98.
Carrara, P.E., 1987. Holocene and latest Pleistocene glacial chronology, Glacier National Park, Montana. Canadian Journal of Earth Sciences 24, 387—395.

Carrara, P.E., McGimsey, R.G., 1981. The late-neoglacial histories of the Agassiz and Jackson glaciers, Glacier National Park, Montana. Arctic and Alpine Research 13, 183—196.
Clague, J.J., Menounos, B., Osborn, G., Luckman, B.H., Koch, J., 2009. Nomenclature and resolution in Holocene glacial chronologies. Quaternary Science Reviews 28, 2231—2238.
Clement, A.C., Seager, R., Cane, M.A., 2000. Suppression of El Nino during the mid-Holocene by changes in the Earth's orbit. Paleoceanography 15, 731—737.
Davis, P.T., Menounos, B., Osborn, G., 2009. Holocene and latest Pleistocene Alpine glacier fluctuations; a global perspective. Quaternary Science Reviews 28, 2021—2033.
Dean Jr., W.E., 1974. Determination of carbonate and organic matter in calcareous sediments and sedimentary rocks by loss on ignition; comparison with other methods. Journal of Sedimentary Petrology 44, 242—248.
DeMaster, D.J., 1981. The supply and accumulation of silica in the marine environment. Geochimica et Cosmochimica Acta 45, 1715—1732.
Denton, G.H., Karlén, W., 1973. Holocene climatic variations; their pattern and possible cause. Quaternary Research 3, 155—205.
Filippelli, G.M., Souch, C., Menounos, B., Slater-Atwater, S., Jull, A.J.T., Slaymaker, O., 2006. Alpine lake sediment records of the impact of glaciation and climate change on the biogeochemical cycling of soil nutrients. Quaternary Research 66, 158—166.
Gibbons, A.B., Megeath, J.D., Pierce, K.L., 1984. Probability of moraine survival in a succession of glacial advances. Geology 12, 327—330.
Grove, J.M., 2004. Little Ice Ages; Ancient and Modern. Routledge, London, UK.
Hall, M., Fagre, D.B., 2003. Modeled climate-induced glacier change in Glacier National Park, 1850—2100. Bioscience 53, 131—140.
Higgins, R.A., 1998. A tale of mines, prospectors, and native Americans: the making of Glacier National Park. Cultural Resource Management 7, 40—43.
Hofmann, M.H., Hendrix, M.S., 2010. Depositional processes and the inferred history of ice-margin retreat associated with the deglaciation of the Cordilleran Ice Sheet: the sedimentary record from Flathead Lake, northwest Montana, USA. Sedimentary Geology 223, 61—74.
Holzhauser, H., Magny, M., Zumbuehl, H., 2005. Glacier and lake-level variations in west-central Europe over the last 3500 years. Holocene 15, 789—801.
Jóhannesson, T., Raymond, C., Waddington, E., 1989. Time-scale for adjustment of glaciers to changes in mass balance. Journal of Glaciology 35, 355—369.
Kaplan, M.R., Wolfe, A.P., Miller, G.H., 2002. Holocene environmental variability in southern Greenland inferred from lake sediments. Quaternary Research 58, 149—159.
Karlén, W., 1981. Lacustrine sediment studies; a technique to obtain a continuous record of Holocene glacier variations. Geografiska Annaler: Series A: Physical Geography 63, 273—281.
Key, C.H., Fagre, D.B., Menicke, R.K., 2002. Glacier retreat in Glacier National Park, Montana. In: Krimmel, R.M. (Ed.), Glaciers of the Western United States. U. S. Geological Survey, Reston, VA, pp. J329—J381.
Koch, J., Osborn, G.D., Clague, J.J., 2007. Pre-'Little Ice Age" glacier fluctuations in Garibaldi Provincial Park, Coast Mountains, British Columbia, Canada. Holocene 17, 1069—1078.
Leonard, E.M., 1997. The relationship between glacial activity and sediment production; evidence from a 4450-year varve record of neoglacial sedimentation in Hector Lake, Alberta, Canada. Journal of Paleolimnology 17, 319—330.
Leonard, E.M., Reasoner, M.A., 1999. A continuous Holocene glacial record inferred from proglacial lake sediments in Banff National Park, Alberta, Canada. Quaternary Research 51, 1—13.
Livingstone, D.A., 1955. A lightweight piston sampler for lake deposits. Ecology 36, 137—139.
Luckman, B.H., 1995. Calendar-dated, early 'Little Ice Age' glacier advance at Robson Glacier, British Columbia, Canada. Holocene 5, 149—159.
Luckman, B.H., Holdsworth, G., Osborn, G.D., 1993. Neoglacial glacier fluctuations in the Canadian Rockies. Quaternary Research 39, 144—153.
MacGregor, K.R., Riihimaki, C.A., Myrbo, A., Shapley, M.D., Jankowski, K., 2011. Geomorphic and climatic change over the past 12,900 yr at Swiftcurrent Lake, Glacier National Park, Montana, USA. Quaternary Research 75, 80—90.
MacLeod, D.M., Osborn, G., Spooner, I., 2006. A record of post-glacial moraine deposition and tephra stratigraphy from Otokomi Lake, Rose Basin, Glacier National Park, Montana. Canadian Journal of Earth Sciences 43, 447—460.
Matthes, F.E., 1942. Report of the committee on glaciers, 1941—42. Transactions — American Geophysical Union, 374—392.
Matthes, F.E., 1940. Report of the committee on glaciers, 1939—40. Transactions — American Geophysical Union, 396—406.
Matthews, J.A., Berrisford, M.S., Quentin Dresser, P., Nesje, A., Olaf Dahl, S., Elisabeth Bjune, A., Bakke, J., John, H., Birks, B., Lie, Ø., 2005. Holocene glacier history of Bjørnbreen and climatic reconstruction in central Jotunheimen, Norway, based on proximal glaciofluvial stream-bank mires. Quaternary Science Reviews 24, 67—90.
Mayewski, P.A., Rohling, E.E., Stager, C.J., Karlen, W., Maasch, K.A., Meeker, L.D., Meyerson, E.A., Gasse, F., van Kreveld, S., Holmgren, K., Lee-Thorp, J., Rosqvist, G., Rack, F., Staubwasser, M., Schneider, R.R., Steig, E.J., 2004. Holocene climate variability. Quaternary Research 62, 243—255.
McCabe, G.J., Fountain, A.G., Dyurgerov, M., 2000. Variability in winter mass balance of Northern Hemisphere glaciers and relations with atmospheric circulation. Arctic, Antarctic, and Alpine Research 32, 64—72.
Menounos, B., 1997. The water content of lake sediments and its relationship to other physical parameters: an alpine case study. The Holocene 7, 207—212.

Menounos, B., Clague, J.J., 2008. Reconstructing hydro-climatic events and glacier fluctuations over the past millennium from annually laminated sediments of Cheakamus Lake, southern Coast Mountains, British Columbia, Canada. Quaternary Science Reviews 27, 701–713.

Menounos, B., Clague, J.J., Osborn, G., Luckman, B.H., Lakeman, T.R., Minkus, R., 2008. Western Canadian glaciers advance in concert with climate change circa 4.2 ka. Geophysical Research Letters 35, L07501.

Menounos, B., Koch, J., Osborn, G., Clague, J.J., Mazzucchi, D., 2004. Early Holocene glacier advance, southern Coast Mountains, British Columbia, Canada. Quaternary Science Reviews 23, 1543–1550.

Menounos, B., Osborn, G., Clague, J.J., Luckman, B.H., 2009. Latest Pleistocene and Holocene glacier fluctuations in Western Canada. Quaternary Science Reviews 28, 2049–2074.

Nesje, A., 2009. Latest Pleistocene and Holocene alpine glacier fluctuations in Scandinavia. Quaternary Science Reviews 28, 2119–2136.

Nesje, A., Matthews, J.A., Dahl, S.O., Berrisford, M.S., Andersson, C., 2001. Holocene glacier fluctuations of Flatebreen and winter-precipitation changes in the Jostedalsbreen region, western Norway, based on glaciolacustrine sediment records. Holocene 11, 267–280.

Nussbaumer, S.U., Steinhilber, F., Trachsel, M., Breitenmoser, P., Beer, J., Blass, A., Grosjean, M., Hafner, A., Holzhauser, H., Wanner, H., 2011. Alpine climate during the Holocene: a comparison between records of glaciers, lake sediments and solar activity. Journal of Quaternary Science, 703–713.

Oerlemans, J., 2005. Extracting a climate signal from 169 glacier records. Science 308, 675–677.

Osborn, G., Menounos, B., Ryane, C., Riedel, J., Clague, J.J., Koch, J., Clark, D., Scott, K., Davis, P.T., 2012. Latest Pleistocene and Holocene glacier fluctuations on Mount Baker, Washington. Quaternary Science Reviews 49, 33–51.

Pederson, G., Whitlock, C., Watson, E., Luckman, B., Graumlich, L., Prato, T., Fagre, D., 2006. Paleoperspectives on climate and ecosystem change. In: Prato, T., Fagre, D.B. (Eds.), Sustaining Rocky Mountain Landscapes: Science, Policy and Management for the Crown of the Continent Ecosystem. Resources for the Future, Washington, D.C, pp. 151–170.

Pederson, G.T., Fagre, D.B., Gray, S.T., Graumlich, L.J., 2004. Decadal-scale climate drivers for glacial dynamics in Glacier National Park, Montana, USA. Geophysical Research Letters 31, L12203.

Ramsey, C.B., 2006. Development of the radiocarbon calibration program Oxcal. Radiocarbon 43, 355–363.

Reasoner, M.A., Osborn, G., Rutter, N.W., 1994. Age of the Crowfoot advance in the Canadian Rocky Mountains: a glacial event coeval with the Younger Dryas oscillation. Geology 22, 439–442.

Reasoner, M.M.A., 1993. Equipment and procedure improvements for a lightweight, inexpensive, percussion core sampling system. Journal of Paleolimnology 8, 273–281.

Refsnider, K.A., Brugger, K.A., 2007. Rock glaciers in central Colorado, USA, as indicators of Holocene climate change. Arctic, Antarctic, and Alpine Research 39, 127–136.

Reimer, P.J., Baillie, M.G.L., Bard, E., Bayliss, A., Beck, J.W., Blackwell, P.G., Ramsey, C.B., Buck, C.E., Burr, G.S., Edwards, R.L., Friedrich, M., Grootes, P.M., Guilderson, T.P., Hajdas, I., Heaton, T.J., Hogg, A.G., Hughen, K.A., Kaiser, K.F., Kromer, B., McCormac, F.G., Manning, S.W., Reimer, R.W., Richards, D.A., Southon, J.R., Talamo, S., Turney, C.S.M., van der Plicht, J., Weyhenmeyer, C.E., 2009. IntCal09 and Marine09 radiocarbon age calibration curves, 0–50,000 years cal BP. Radiocarbon 51, 1111–1150.

Reyes, A.V., Wiles, G.C., Smith, D.J., Barclay, D.J., Allen, S., Jackson, S., Larocque, S., Laxton, S., Lewis, D., Calkin, P.E., Clague, J.J., 2006. Expansion of alpine glaciers in Pacific North America in the first millennium A.D. Geology 34, 57–60.

Ryder, J.M., Thomson, B., 1986. Neoglaciation in the southern Coast Mountains of British Columbia; chronology prior to the late Neoglacial maximum. Canadian Journal of Earth Sciences 23, 273–287.

Schaefer, J.M., Denton, G.H., Kaplan, M., Putnam, A., Finkel, R.C., Barrell, D.J.A., Andersen, B.G., Schwartz, R., Mackintosh, A., Chinn, T., Schluechter, C., 2009. High-frequency Holocene glacier fluctuations in New Zealand differ from the northern signature. Science 324, 622–625.

Selkowitz, D.J., Fagre, D.B., Reardon, B.A., 2002. Interannual variations in snowpack in the Crown of the Continent ecosystem. Hydrological Processes 16, 3651–3665.

Strickland, J.D.H., Parsons, T.R., 1965. A manual of sea water analysis; with special reference to the more common micronutrients and to particulate organic material. Fisheries Research Board of Canada Report 125, 203.

Stuiver, M., Reimer, P.J., 1993. Extended ^{14}C data base and revised CALIB 3.0 ^{14}C age calibration program. Radiocarbon 35, 215–230.

Viau, A.E., Gajewski, K., Fines, P., Atkinson, D., Sawada, M.C., 2002. Widespread evidence of 1500 yr climate variability in North America during the past 14 000 yr. Geology 30, 455–458.

Wanner, H., Beer, J., Buetikofer, J., Crowley, T.J., Cubasch, U., Flueckiger, J., Goosse, H., Grosjean, M., Joos, F., Kaplan, J.O., Kuettel, M., Mueller, S.A., Prentice, I.C., Solomina, O., Stocker, T.F., Tarasov, P., Wagner, M., Widmann, M., 2008. Mid- to late Holocene climate change; an overview. Quaternary Science Reviews 27, 1791–1828.

Wanner, H., Solomina, O., Grosjean, M., Ritz, S.P., Jetel, M., 2011. Structure and origin of Holocene cold events. Quaternary Science Reviews 30, 3109–3123.

Whipple, J.W., 1992. Geologic map of Glacier National Park, Montana. USGS Miscellaneous Investigations Series. I-1508-F, 1:100,000.

Zdanowicz, C.M., Zielinski, G.A., Germani, M.S., 1999. Mount Mazama eruption; calendrical age verified and atmospheric impact assessed. Geology 27, 621–624.